

# 2.4

## *Anderson Localization of Light in Layered Dielectric Structures*

**Yury Bliokh**

*Technion—Israel Institute of Technology*

**Konstantin Y. Bliokh**

*National University of Ireland*

**Valentin Freilikher**

*Bar-Ilan University*

**Franco Nori**

*Advanced Science Institute, RIKEN*

*University of Michigan*

### CONTENTS

2.4.1	Introduction .....	56
2.4.2	Lyapunov Exponent, Localization, and Transmission Lengths .....	58
2.4.3	Statistics of the Transmission in 1D Disordered Systems .....	61
2.4.3.1	Transport and Localization in Randomly Layered Media .....	61
2.4.3.1.1	Normal Incidence: Transfer Matrix Method .....	61
2.4.3.1.2	Oblique Incidence: Reduction to the Oscillatory Problem .....	62
2.4.3.2	Transport and Localization in Continuous Active Media .....	62
2.4.3.2.1	Invariant Embedding Method .....	62
2.4.3.3	Transport and Localization in 1D Periodic Structures with Disorder .....	64
2.4.4	Disorder-Induced Resonances in 1D Systems .....	65
2.4.4.1	Exploration by Analogy: Deterministic Model of Random Resonances ....	65
2.4.4.2	How Is an Effective Cavity Built Up? .....	71
2.4.4.3	Coupling and Level Repulsion .....	72
2.4.4.4	Bistability of Anderson Localized States in Nonlinear Random Media ....	75
2.4.5	Experimental Studies of Resonances .....	77
2.4.5.1	Inverse Scattering Problems and Remote Sensing of Disordered Samples .....	80
2.4.6	Anderson Localization in Exotic Materials .....	81
2.4.6.1	Suppression of Anderson Localization in Disordered Metamaterials .....	81
2.4.6.2	Transport and Localization in Disordered Graphene Superlattices .....	82
2.4.7	Conclusion .....	83
	Acknowledgments .....	84
	References .....	84

---

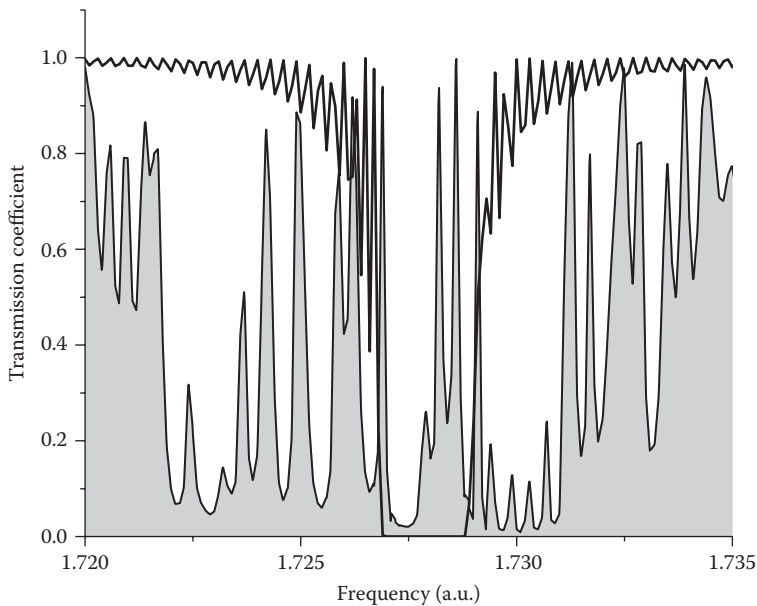
### 2.4.1 Introduction

Wave propagation in disordered media is a rich and long-standing problem that attracts many efforts, both theoretical and experimental. After almost a century of a complete sway of radiative transport and diffusion approaches, it recently became clear that the interference of multiply-scattered fields (which is neglected in classical diffusion theory) dramatically affects all wave processes, especially in systems with fluctuations. The most startling manifestation of this effect is the strong localization of electromagnetic radiation in weakly-disordered random media. Since Anderson's seminal paper,<sup>1</sup> localization has attracted ever-increasing attention from physicists and engineers. Without attempting an exhaustive review of available literature we note that the bibliography related to this rather young area already numbers in hundreds of original articles, reviews, and books (see, e.g., the review,<sup>2</sup> the monographs,<sup>3</sup> and references therein). Worthy of notice are the great number of meetings dedicated to the 50 years' anniversary of Anderson localization (half-a-year non-stop workshop in Cambridge, conferences in Paris, Dresden, Santa Barbara, etc.) where physicists, mathematicians, chemists, engineers, biologists, and even economists not only presented a plethora of new results but also formulated a great many challenging questions.

A boost to the studies of Anderson localization in disordered optical and quantum systems was given recently by the creation of new materials with unique properties that have spurred the rise of new conceptual challenges and high-tech applications. The most impressive latest examples include photonic crystals, plasmonics, left-handed metamaterials, Bose–Einstein condensates, and graphene. Yet it should be remembered that most of the prospects for potential technological use of these materials rest on the predicted properties of ideal (e.g., perfectly periodic) systems. Even a small amount of disorder, however, which is inevitably present in any real sample, could affect its properties dramatically (see [Figure 2.4.1](#)). Therefore, when it comes to real applications, a comprehensive study of the effects of disorder is a must. Moreover, these investigations are of interest by itself because strongly disordered (with no periodic component) systems possess further unexpected physical properties, which make them potentially useful as an alternative to the pure periodic configurations.

One-dimensional (1D) strong localization has received the most study, both analytically and numerically. In particular, the localization of the eigenstates in closed 1D disordered systems and the exponentially small (with respect to the length) transparency of open systems with 1D disorder have been scrutinized with mathematical rigor (e.g., see Ref. 4 and references therein).

The most common physical manifestation of localization is the fact that sheets of perfectly transparent paper stacked together in large numbers reflect light as a good mirror.<sup>5</sup> Much less evident (though long predicted theoretically<sup>6</sup>) is that for each sufficiently long disordered 1D sample, there exists a random set of frequencies that go all the way through the sample almost unreflected, that is, with the transmission coefficient close to unit. High transparency is always accompanied by a relatively large concentration (localization) of energy around randomly located points inside the system. Along with these “classical” trademarks of strong localization there is a plethora of not-less-amazing effects that disorder can set up in one dimension. Examples are: random lasing,<sup>7,8</sup> critical coupling,<sup>9</sup> necklace states,<sup>10,11</sup> level crossing and repulsion,<sup>9</sup> slow light and superluminal group velocities,<sup>12</sup> bistability and nonreciprocity of resonant transmission in nonlinear random media,<sup>13</sup> delocalization in metamaterials,<sup>14–16</sup> and in graphene superlattices,<sup>17</sup> and so on.

**FIGURE 2.4.1**

Transmission spectra of a regular periodic sample (thick black line) and of a sample whose period fluctuates in the range of 1%.

Although, generally, a disordered 1D system is a mathematical abstraction, it can provide an adequate model for many actual physical objects. For example, randomly stratified media are found in numerous geological and biological settings, as well as in fabricated materials. Interference of waves in such systems determines the transport of seismic waves in the earth's crust and sonic waves in the oceans; reflection and transmission from multilayer dielectric stacks used as optical reflectors, filters, and lasers; propagation and localization in single-mode optical fibers and microwave waveguides, etc. Even more important, it may be possible to utilize highly disordered samples for many applications. For instance, tunable switches or narrow-line laser sources can be created using randomly stacked systems.

Although the strong localization of waves in 1D random media has been well studied theoretically, most of the analytical results have been obtained for values averaged over ensembles of random realizations. These results are physically meaningful for the self-averaging Lyapunov exponent (inverse localization length), which becomes nonrandom in the macroscopic limit. For non-self-averaging quantities (field amplitude and phase, intensity, transmission and reflection coefficients, etc.), a system of any size is always mesoscopic, and, therefore, mean values have little to do with the measurements at individual (usually small in number) samples. This is most pronounced when it comes to disorder-induced resonances whose parameters are extremely sensitive to the fine structure of a particular sample and strongly fluctuate from realization to realization. In particular, the ensemble averaging wipes out all information about the frequencies and locations of individual localized states within a particular sample, even though just this set of data is essential for applications. Another frustrating inconsistency between most of the existing theories and measurements is that in real systems, losses (absorption and leakage) are inevitably present, whereas mathematicians and theoreticians usually prefer lossless (Hermitian) models that are much easier to deal with.

In this chapter, we present a brief overview of methods and results regarding the transport and localization in disordered 1D systems, followed by a detailed description of the current state-of-the-art in theoretical and experimental studies of the resonant properties of randomly layered media.

## 2.4.2 Lyapunov Exponent, Localization, and Transmission Lengths

Consider the 1D Helmholtz equation

$$u''(x) + k^2[\epsilon_0 + \delta\epsilon(x)]u(x) = 0 \quad (2.4.1)$$

with the self-adjointed (currentless) boundary condition at a point  $x_0$

$$u(x_0) + au'(x_0) = 0, \quad (2.4.2)$$

where  $a$  is any real number. It is easy to show that Equation 2.4.2 means that the modulus of the reflection coefficient from the point  $x_0$  equals to one. The functions  $\xi$  and  $\varphi$  determined as

$$\begin{aligned} u(x) &= e^{\xi(x,k)} \sin \varphi(x,k), \\ u'(x) &= ke^{\xi(x,k)} \cos \varphi(x,k) \end{aligned} \quad (2.4.3)$$

satisfy the following (nonlinear) equations:

$$\begin{aligned} \varphi'(x,k) &= k[1 - \delta\epsilon(x)\sin^2 \varphi(x,k)] \\ \xi(x,k) &= \xi(0,k) + \frac{k}{2} \int_0^x \delta\epsilon(y) \sin 2\varphi(y,k) dy. \end{aligned} \quad (2.4.4)$$

Assuming that  $\delta\epsilon(x)$  is a statistically homogeneous random function with zero average,  $\langle \delta\epsilon(x) \rangle = 0$ , and disappearing at infinity correlations,  $W(x) = \langle \delta\epsilon(0)\delta\epsilon(x) \rangle_{x \rightarrow \infty} \rightarrow 0$ , the following statement is true:<sup>4</sup> in the limit  $|x| \rightarrow \infty$ , the ratio  $\xi(x,k)/x$  approaches a non-random limit that is positive for all  $k$ :

$$\lim_{|x| \rightarrow \infty} \frac{\xi(x,k)}{x} = \lim_{|x| \rightarrow \infty} \left\langle \frac{\xi(x,k)}{x} \right\rangle \equiv \gamma(k) > 0. \quad (2.4.5)$$

In principle, this result follows from the Furstenberg theorem,<sup>18</sup> which holds that, under some conditions, the specific logarithm of the product of  $N$  transfer matrices  $M_j$  tends to a positive limit as  $N$  goes to infinity:

$$\lim_{N \rightarrow \infty} \left( \frac{1}{N} \ln \prod_{j=1}^N M_j \right) = \mu > 0.$$

Equation 2.4.5 presents two fundamental properties of a 1D random system satisfying the above-listed conditions:

1. The Lyapunov exponent,  $\gamma(k)$ , is a self-averaging quantity; that is, at any single random realization it tends to the ensemble-averaged nonrandom mean value when the size of the realization increases infinitely.
2. For a single random realization, the amplitude of the wave function increases exponentially with nonrandom increment  $\gamma(k)$  on both sides of the point, at which the currentless boundary condition (2.4.2) holds.

The inverse of the Lyapunov exponent

$$l_{\text{loc}} = \frac{1}{2\gamma} \quad (2.4.6)$$

is called the localization length. The meaning of this term becomes clear if one considers two solutions of Equation 2.4.1,  $u_1(x)$  and  $u_2(x)$ , in the interval  $0 \leq x \leq L$  (closed 1D system), each satisfying the boundary condition (2.4.2) at  $x = 0$  and  $x = L$ , respectively, and therefore each increasing exponentially away from these points. An eigenfunction,  $\psi_n(x)$ , of this system can be constructed from  $u_1(x)$  and  $u_2(x)$  under the condition that these functions and their derivatives match at some point  $x_n$  inside the interval. Obviously, an eigenfunction,  $\psi_n(x)$ , obtained in this way is localized; that is, its envelop,  $A^2(x)$ , decreases exponentially on both sides of  $x_n$ :

$$A^2(x) \equiv \left[ |u(x)|^2 + \frac{1}{k^2} |u'(x)|^2 \right] \sim \exp\left(-\frac{|x - x_n|}{l_{\text{loc}}}\right) \quad (2.4.7)$$

In the case of the white-noise disorder [ $\delta\varepsilon(x)$  is a  $\delta$ -correlated random process], the closed Fokker–Planck equation for the probability density distribution,  $P(\xi, z)$ , of the quantity  $\xi(x)$  can be derived and solved using an averaging over rapid random phase.<sup>4,19</sup> This is impossible if  $\delta\varepsilon(x)$  has a finite correlation radius, and the random-phase approximation breaks down (as well as the single-parameter scaling theory of localization). In this case, the ordered cumulant method of Van-Kampen can be used to obtain the weak disorder expansion of the Lyapunov exponent  $\gamma(k)$ .<sup>20</sup> The first term of this expansion can be obtained from Equation 2.4.4 by solving the equation for the phase perturbatively and substituting the result into the integral for  $\xi(x, k)$ . The limit  $|x| \rightarrow \infty$  yields the famous result

$$\gamma(k) = \frac{k^2}{4} \int_0^\infty dx W(x) \cos 2kx, \quad (2.4.8)$$

which means that the localization is due to the resonant Bragg backscattering provided by the  $2k$  Fourier component of the random potential. Higher orders of the weak disorder expansion have been calculated and can be found in the literature.<sup>20,21</sup>

The notion of the Lyapunov exponent is related to the eigenvalues boundary problem, and therefore is well defined only for closed disordered systems. From the physical point of view, not less relevant is the scattering problem that addresses the transmission, reflection, and propagation in open structures with fluctuating parameters.

Transport properties of a 1D system of a finite length  $L$  can be described by the transfer matrix  $\hat{M}$ , which relates the amplitudes of the incident ( $A_L$ ) and outgoing ( $B_L$ ) waves on one side of the sample to those on the other side ( $A_R$  and  $B_R$ ):

$$\begin{pmatrix} B_R \\ A_R \end{pmatrix} = \hat{M} \begin{pmatrix} B_L \\ A_L \end{pmatrix} \quad (2.4.9)$$

Assuming time-reversal invariance, the transfer matrix  $\hat{M}$  can be written as

$$\hat{M} = \begin{vmatrix} \frac{1}{t^*} & -\left(\frac{r}{t}\right)^* \\ -\left(\frac{r}{t}\right) & \frac{1}{t} \end{vmatrix} = \frac{1}{\sqrt{T}} \begin{vmatrix} e^{i\phi_t} & -\sqrt{1-T} e^{-i(\phi_r - \phi_t)} \\ -\sqrt{1-T} e^{i(\phi_r - \phi_t)} & e^{-i\phi_t} \end{vmatrix}, \quad (2.4.10)$$

where  $t = \sqrt{T} \exp(i\phi_t)$ , and  $r = \sqrt{1-T} \exp(i\phi_r)$  are the transmission and reflection amplitudes, respectively;  $T \equiv |t|^2$  is the transmission coefficient. In what follows, the quantity  $l_{\text{tr}}(L) = \left[-\frac{1}{2L} \ln T(L)\right]^{-1}$  is called the transmission length.

Evidently, the solution of the boundary value problem (2.4.1), (2.4.2) and the solution of the scattering problem in the limit  $L \rightarrow \infty$  are uniquely related; that is,

$$\begin{pmatrix} u(L) \\ u'(L) \end{pmatrix} = \hat{M}' \begin{pmatrix} u(0) \\ u'(0) \end{pmatrix}$$

where  $\hat{M}'$  is an elementary linear transformation of the transfer matrix  $\hat{M}$ .

When the size  $L$  of the system is much larger than the localization length  $l_{\text{loc}}$ , the transmission coefficient  $T$  becomes exponentially small (with the probability exponentially close to one), and statistically independent of the phases  $\phi_t$  and  $\phi_r$ . As a result, each matrix  $\hat{M}$  and  $\hat{M}'$  factorizes into a product of a large factor  $1/\sqrt{T}$  and a matrix of the order of unity, which is statistically independent of  $T$ . This means that, asymptotically for large  $L$ , one can write

$$\gamma(k) = \frac{1}{2L} \ln \left[ |u(L)|^2 + \frac{1}{k^2} |u'(L)|^2 \right] = -\frac{1}{2L} \ln T(L) + O(L^0), \quad (2.4.11)$$

where the second term in the asymptotic expansion is independent of the first one, and their cumulants are of the order of unity. Apparently, in the limit  $L \rightarrow \infty$ , the transmission length coincides with the inverse Lyapunov exponent (localization length):

$$l_{\text{tr}} = l_{\text{loc}}. \quad (2.4.12)$$

This fact is generally recognized. However, it was shown recently<sup>14</sup> that, surprisingly enough,  $l_{\text{loc}}$  and  $l_{\text{tr}}$  can be different in stacks made of alternating right- and left-handed dielectric layers with random refractive indices and thicknesses.

The equality Equation 2.4.12 means, in particular, that the localization length can be probed noninvasively from the transmission coefficient, without measurements of the field amplitude inside random samples.

### 2.4.3 Statistics of the Transmission in 1D Disordered Systems

#### 2.4.3.1 Transport and Localization in Randomly Layered Media

##### 2.4.3.1.1 Normal Incidence: Transfer Matrix Method

One of the most efficient theoretical methods of studying general properties of transmission in 1D disordered systems is based on the composition rule for a chain of statistically identical and independent random scatterers.<sup>22</sup> For stratified media, the method is straightforward and involves the calculation of the transfer matrix  $\hat{M}$  using the following exact recurrence relations for the transmission coefficients (for details, see Ref. 14 and references therein):

$$T_n = \frac{T_{n-1}t_n}{1 - R_{n-1}r_n}, \quad (2.4.13)$$

$$R_n = r_n + \frac{R_{n-1}t_n^2}{1 - R_{n-1}r_n} \quad (2.4.14)$$

Here  $T_n$  and  $R_n$  are, respectively, the total transmission and reflection coefficients of a stack of  $n$  layers,  $t_n$  and  $r_n$  are the (complex) transmission and the reflection amplitudes of a single layer. Equations 2.4.13 and 2.4.14 are general and, taking into account all multiply-scattered fields, present exact solutions that can be used for direct numerical simulations.

For a sample composed of  $N$  statistically identical and independent random layers of normal (with positive refractive index) dielectrics, the following expression for the average inverse transmission length can be derived from Equations 2.4.13 and 2.4.14:<sup>14</sup>

$$\left\langle \frac{1}{l_{\text{tr}}(N)} \right\rangle = \frac{1}{l_{\text{loc}}} + \frac{1}{Nd} \text{Re} \left[ \langle r \rangle^2 \frac{1 - \langle t^2 \rangle^N}{(1 - \langle t^2 \rangle)^2} \right], \quad (2.4.15)$$

where  $d$  is the average width of the layers, and the inverse localization length is

$$\frac{1}{l_{\text{loc}}} = \frac{1}{l_{\text{tr}}(\infty)} = -\langle \ln |t| \rangle - \text{Re} \frac{\langle r \rangle^2}{1 - \langle t^2 \rangle}. \quad (2.4.16)$$

Note that when  $N \rightarrow \infty$ , Equation 2.4.15 transforms into Equation 2.4.12, that is, the localization and transmission lengths become equal.

In the case of weak scattering, the reflection from a single layer is small,  $|r_n| \ll 1$  and Equation 2.4.16 yields:

$$l_{\text{loc}} = \begin{cases} \frac{12d}{\delta^2}, & \lambda = 2\pi/k \rightarrow 0, \\ \frac{3\lambda^2 d}{2\pi^2 \delta^2}, & \lambda = 2\pi/k \rightarrow \infty. \end{cases} \quad (2.4.17)$$

In the derivation of Equation 2.4.17, it was assumed that the width of each layer was distributed uniformly over the interval  $[d - \delta, d + \delta]$ , and the refractive index did not fluctuate. Nevertheless, the functional  $\lambda$ -dependences, Equation 2.4.17, of the localization length in weakly disordered systems are rather general (e.g., see Ref. 23).

#### 2.4.3.1.2 Oblique Incidence: Reduction to the Oscillatory Problem

An original efficient method of calculating the localization length was developed in Ref. 24. It uses the fact that the reflection from an adequately long, randomly layered sample differs from unity by an exponentially small number,  $1 - R(L) \sim \exp(-L/l_{\text{loc}})$ , and, therefore, the flux along the system is also exponentially small. This *a priori* information enables one to assume (with an exponential accuracy) that the field in each layer inside the sample is a standing wave, and to reduce the wave propagation problem to the oscillatory one, with the real-valued wave amplitude being a single unknown. This simplifies the problem significantly as compared to the conventional transfer matrix method, where the evolution of two independent waves in each layer is considered. Using this method, the oblique incidence of electromagnetic waves on a randomly layered medium was studied.<sup>24</sup> Two effects not found at normal incidence were predicted: dependence of the localization length on the polarization and the decrease of the localization length as a result of the internal reflections from layers with small refractive indices. The attenuation rate for *p*-polarized radiation is shown to be always smaller than that of *s*-polarized waves, which is to say that an adequately long, randomly layered sample polarizes transmitted radiation. The localization length for *p*-polarization depends nonmonotonically on the angle of propagation and, under certain conditions, turns to infinity at some angle, which means that typical (non-resonant) random realizations become transparent at this angle of incidence (stochastic Brewster effect).

### 2.4.3.2 Transport and Localization in Continuous Active Media

#### 2.4.3.2.1 Invariant Embedding Method

An alternative approach to the 1D random scattering problem is the invariant embedding method,<sup>25</sup> which amounts to finding the solution of the following system of (exact) first-order Langevin-type equations for the reflection and transmission coefficients:

$$\frac{dr(L)}{dL} = \frac{i}{2} k \epsilon(L) [e^{-ikL} + r(L)e^{ikL}]^2 \quad (2.4.18)$$

$$\frac{dt(L)}{dL} = \frac{i}{2} k \epsilon(L) t(L) [e^{-ikL} + r(L)e^{2ikL}] \quad (2.4.19)$$

Equations 2.4.18 and 2.4.19 can be treated statistically by means of exact numerical calculations and approximate analytical methods as well. A Fokker–Planck equation can be derived, which, in the case of the white-noise disorder, yields the distribution function for the reflection coefficient  $R(L) = |r(L)|^2$ . In the absence of absorption or amplification, this distribution function provides complete information on the transmission coefficient  $T = |t(L)|^2$ .

The problem becomes much more complicated in the case of lossy media where the energy conservation law not only connects  $T$  and  $R$  but also involves a random amount of the absorbed intensity. In the paper,<sup>26</sup> the asymptotically exact expressions for all moments of the transmission coefficient have been obtained by mapping the Fokker–Planck problem onto a Schrödinger equation with imaginary time. In particular, it has been shown that in the case of small absorption,  $l_{\text{loc}} \ll l_a$  ( $l_a$  is the absorption length),

$$-\frac{\ln \langle T(L) \rangle}{L} = \left( \frac{1}{4l_{\text{loc}}} + \frac{1}{l_{\text{in}}} \right), \quad (2.4.20)$$

where

$$l_{\text{in}} = l_{\text{loc}} \ln^2 \left( \frac{l_a}{l_{\text{loc}}} \right) \quad (2.4.21)$$

is a disorder-induced absorption length, which lies between the localization and absorption lengths, see Ref. 26

$$l_{\text{loc}} \ll l_{\text{in}} \ll l_a.$$

This means that in the localized regime, the disorder causes drastic enhancement of the attenuation of the average transmission coefficient as compared to that in the corresponding pure ( $\delta\varepsilon = 0$ ) sample ( $l_{\text{in}} \ll l_a$ ). Note that the disorder-induced absorption length for the localized waves, Equation 2.4.21, is also significantly smaller (i.e., the effect of absorption is much stronger) than that in the diffusive regime:  $l_{\text{in}} \ll \sqrt{l_{\text{loc}} l_a}$ .

In contrast to Equation 2.4.20, the contributions from scattering and absorption to the average decrement of the transmission coefficient (or to the Lyapunov exponent) are additive:

$$-\left\langle \frac{\ln T(L)}{L} \right\rangle = \left( \frac{1}{l_{\text{loc}}} + \frac{1}{l_a} \right) > -\frac{\ln \langle T(L) \rangle}{L}. \quad (2.4.22)$$

It can be shown that  $\ln \langle T(L) \rangle$  and  $\langle \ln T(L) \rangle$  are different not only in lossy media (compare Equations 2.4.20 and 2.4.22) but also in nonabsorbing ( $l_a \rightarrow \infty$ ) systems. This is because  $\ln T(L)/L$  is a self-averaging quantity (see Equations 2.4.8 and 2.4.11), with very narrow distribution ( $\delta$  function at  $L \rightarrow \infty$ ) centered at its mean value. This means that at a randomly chosen realization,  $\ln T(L)$  will be found in a small vicinity of its average value with a probability exponentially close to one, and therefore the value of a function  $F[\ln T(L)]$  will be close to  $F[\langle \ln T(L) \rangle]$  with the same probability. In particular, the transmission coefficient typically is exponentially small:

$$T_{\text{typ}}(L) = \exp \left[ \frac{\ln \langle T(L) \rangle}{L} \right] = \exp \left[ -L \left( \frac{1}{l_{\text{loc}}} + \frac{1}{l_a} \right) \right]. \quad (2.4.23)$$

On the other hand,  $T(L)$  itself is a strongly fluctuating random variable with broad distribution. It turns out that the main contribution to its average value comes not from the typical (nontransparent) realizations but from low-probable ones, so-called resonant realizations (see Section 2.4.4), corresponding to the non-Gaussian tail of the distribution of  $\ln T$ , where the transmission coefficient is of the order of unity. This is due to these resonantly transparent realizations that the average transmission is much larger than the typical one. For example,<sup>4</sup> in the lossless media with delta-correlated disorder

$$\frac{\langle T(L) \rangle}{T_{\text{typ}}(L)} = \exp\left(\frac{3}{4} \frac{L}{l_{\text{loc}}}\right) \gg 1.$$

while both  $T_{\text{typ}}(L)$  and  $\langle T(L) \rangle$  are exponentially decaying functions of  $L$  (the difference is in the attenuation rate). More than that, there are quantities for which the typical and mean values have completely different functional dependencies. An example of how misleading a formally calculated mean value can be is the energy flux,  $J = 2\text{Im}(u^*u')$ , created by a point source located at the perfectly reflecting edge ( $x = 0$ ) of a disordered sample of length  $L$ . As shown in Ref. 2, the mean flux does not interact with disorder and is equal to its value in the homogeneous sample:  $\langle J(L) \rangle = 2/k$ . This result is physically meaningless because to obtain it experimentally, averaging over an exponentially large number of realizations is necessary. At the same time, the measurement at a single random sample will give (with a probability exponentially close to unity) the typical value, which is exponentially small as a result of the localization effect:  $J_{\text{typ}} = \exp(\langle \ln J \rangle) \sim \exp(-L/l_{\text{loc}})$ . This is because  $\ln J$  is an additive self-averaging quantity.

The typical-medium approach in the theory of Mott–Anderson localization in electron systems is discussed in Ref. 27.

An outstanding distinction between the transmission at typical and resonant configurations of amplifying random media has been found in Ref. 28. It has been shown that in random systems with complex dielectric permittivity,  $\varepsilon(x) = \varepsilon_0 + \delta\varepsilon(x) + i\Gamma$ , the inverse Lyapunov exponent is always negative, independent of the sign of  $\Gamma$ ;<sup>29</sup> that is, the typical transmission through a finite disordered dielectric sample is exponentially small for both absorbing and amplifying disordered samples. To the contrary, the mean value of the transmission coefficient in random media with gain ( $\Gamma > 0$ ) diverges (because of the infinitely increasing resonant intensity) even at samples of finite size. To obtain physically meaningful finite values of the transmission, the nonlinear effect of saturation should be included in the model.

### 2.4.3.3 Transport and Localization in 1D Periodic Structures with Disorder

The study of the effects of disorder on the wave properties of periodic structures is essential for better understanding the physics of the interplay between periodicity and disorder, and also for practical applications. Indeed, though considerable effort has been expended to develop highly periodic structures, deviations from periodicity inevitably present in any manufactured photonic crystal can significantly modify its optical characteristics. To reveal the most general transport properties of disordered 1D structures that are periodic on average (1D photonic crystals), the Helmholtz Equation 2.4.1 can be used, in which  $\varepsilon_0$  is a periodic function of the coordinate  $x$ , and  $\langle \delta\varepsilon(x) \rangle = 0$ . Three types of periodic systems with weakly-perturbed periodicity were studied in Ref. 30: (i) stacks of alternating discrete dielectric layers with constant permittivities,  $\varepsilon^{(1)}$  and  $\varepsilon^{(2)}$ , and fluctuating width of each layer,  $d_i = d + \delta d_i$ ; (ii) samples of the same geometry but with constant  $d_i = d$  and

$\epsilon_{2i-1}^{(1)} = \epsilon_0^{(1)} + \delta\epsilon_{2i-1}$ ,  $\epsilon_{2i}^{(2)} = \epsilon_0^{(2)} + \delta\epsilon_{2i}$ ; (iii) continuous periodic media with  $\epsilon(x) = A\cos qx + \delta\epsilon(x)$ . The quantities  $\delta d_i$ ,  $\delta\epsilon_i$ , and  $\delta\epsilon$  are assumed to be random variables with known statistics. For numerical simulations of the propagation in discrete systems (i) and (ii), the transfer matrix approach (Section 2.4.3.1) is appropriate, whereas for the continuous model (iii), the invariant embedding method (Section 2.4.3.2) is best suited.

The following property is found to be universal, independent of the geometry of the system and of the type of disorder for the frequencies of the incident wave belonging to a band gap of the underlying periodic structure, weak disorder enhances (in contrast to homogeneous in average random 1D systems) the transparency. Moreover, the localization length and the transmission coefficient grow when the strength of the disorder increases. This is because in the presence of disorder, the channels of the propagation that are closed in the perfectly periodic system open up as a result of the partial filling of the density of photonic states in the gap by the tails of this density from the transparency zones bordering the gap.

In contrast to the band gap, the features of the transmission for frequencies in the transparency zone depend on the type of disorder. For these frequencies, the surprising non-monotonic dependence of the localization length on the strength of disorder was observed in stratified media with geometrical disorder and constant dielectric permittivities [type (i)]. In such a medium, the initial decrease of the transmission coefficient is a classical manifestation of Anderson localization, which is usually stronger for larger fluctuations (see previous sections). When the fluctuations of the width become adequately large, the decrease gives way to the enhancement of the transmission for increasing disorder. To explain this rather counterintuitive result, we note that in the strong localization regime, the inverse localization length is approximately equal to<sup>30</sup>

$$\frac{1}{l_{\text{loc}}} \approx \langle R_1 \rangle, \quad (2.4.24)$$

where  $R_1$  is the reflection coefficient of a single layer. This means that, in this case, the total transmission of a stack is completely determined by the mean value of the reflection coefficient of a single element. For a dielectric layer,  $R_1$  is a periodic function of the width  $d$  of the layer, and the averaging in Equation 2.4.24 means the integration of  $R_1$  over  $d$  in an interval  $\Delta_d$ , in which the fluctuations  $\delta d_i$  are distributed. Evidently, if the disorder is strong,  $\Delta_d \approx d$ , the increase of the interval of the integration of the periodic function causes a decrease of  $\langle R_1 \rangle$ .

In a system of the second type (random  $\epsilon$ ),  $R_1$  is proportional to  $\delta\epsilon$  and the growth of its variance enhances the strength of a single scattering, leading to a monotonic increase of  $\langle R_1 \rangle$ . On further increase of the disorder, all three types of random systems finally lose all traces of the underlying periodicity, the band structure disappears, and waves of all frequencies experience the same disordered medium that becomes homogeneous in average.

## 2.4.4 Disorder-Induced Resonances in 1D Systems

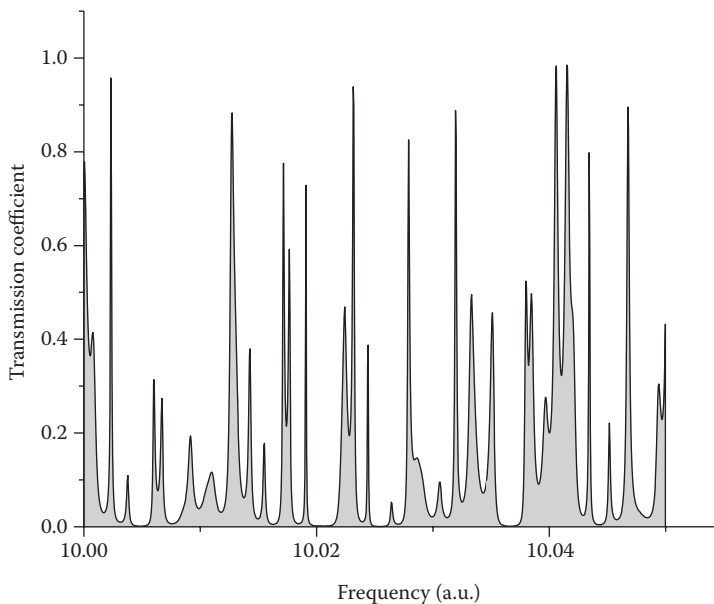
### 2.4.4.1 Exploration by Analogy: Deterministic Model of Random Resonances

As shown in Section 2.4.1, disorder can strongly affect the transport properties of periodic systems, sometimes to the point where the photonic band structure is completely destroyed.

As fluctuations of the dielectric and geometrical parameters are inevitably present in any manufactured periodic sample, this could create a serious obstacle in the efficient practical use of photonic crystals. Therefore, nowadays considerable efforts of researches and producers go into the control of fluctuations. However, if rather than combating imperfections of periodicity, one fabricated highly disordered samples, they could be equally well harnessed, for example, for creating tunable resonant elements. This is because 1D random configurations have a unique band structure that for some applications has obvious advantages over those of photonic crystals.

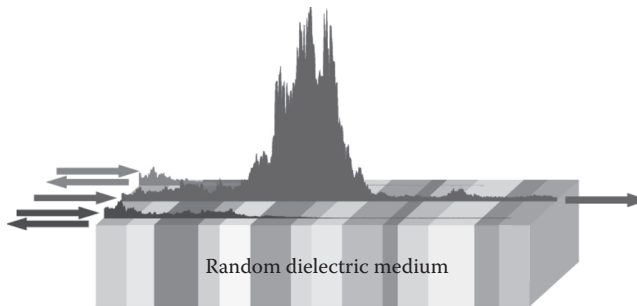
The transparency spectrum of a typical 1D random sample consists of very narrow bands separated by broad gaps (Figure 2.4.2). For adequately long structures, the bands are so narrow that they can be treated as (quasi)-resonances that are well pronounced; that is, their widths are much smaller than the distances between them, both in the frequency domain and in real space. Physically, at each resonant frequency, an open random 1D configuration can be considered as an open resonator with high quality factor. An important advantage of application features of such a system is that, in contrast to a regular resonator whose modes occupy all inner space, in a 1D random structure, each eigenfrequency (mode) is localized inside its own effective “cavity” whose size is much smaller than that of the sample. Figure 2.4.3 shows the intensities of the fields generated by a resonant frequency (central curve), and by two off-resonance, typical frequencies (side curves) with exponentially small transmission coefficients. Another important advantage of disordered samples is that they are much easier to fabricate as they do not require precise periodicity.

The existence of disorder-induced resonances in 1D random media was predicted a while ago.<sup>6</sup> The random set of resonant frequencies is a sort of 1D optical “speckle pattern,” which is individual for each random configuration and represents its unique “fingerprint.”



**FIGURE 2.4.2**

Transmission coefficient  $T$  as a function of the wave frequency.

**FIGURE 2.4.3**

(See color insert.) Amplitude of the field inside the sample as a function of the coordinate for three different wavelengths. (Reprinted with permission from K. Bliokh et al., *Rev. Mod. Phys.* **80**, 1201, 2008. Copyright 2008 by the American Physical Society.)

Although the resonances indirectly manifest themselves in the dominant contribution to the mean transmission coefficient (see Section 2.4.3.2), the ensemble-averaged quantities do not provide any information about the frequencies, locations, and spatial intensity distribution of the individual localized states, yet just this set of data is essential for applications (e.g., random lasing). Unfortunately, an explicit, general analytical solution of Equation 2.4.1 with arbitrary function  $\delta\epsilon(x)$  does not exist, and standard approximate methods (e.g., small perturbations expansion) are of little help, because the adequate description of strong localization calls for the summation of infinite number of multiply-scattered fields. On the other hand, direct optical measurements of the field inside a given disordered sample are generally not feasible.

In such a situation, the question arises as to whether the outgoing radiation bears the necessary information on what happens inside the sample or, more specifically, whether the parameters and internal structure of individual resonances can be retrieved from the standard external measurements of the transmission and reflection amplitudes.

The positive answer to this question is given by means of the approach developed by Bliokh et al.,<sup>31</sup> which is based on the concept that the fundamental properties of resonances are universal and independent of the physical nature of the system, regular or random, whether it is a quantum-mechanical potential well, an optical or microwave resonator, or a 1D random medium.<sup>32</sup> The distinguishing feature of a random structure is that there are no regular walls in it, and the strong reflection that locks the radiation in an effective resonant cavity is the result of Anderson localization. Moreover, different segments of the sample turn out to be transparent for different frequencies; that is, each localized mode is associated with its own resonator.

In the framework of approach,<sup>31</sup> the problem of the transport and localization in a 1D random medium is mapped onto an exactly solvable quantum mechanical problem of tunneling and resonant transmission through an effective deterministic potential. With the formulae derived on the basis of this mapping, the parameters of the individual resonances, in particular, their spectral and spatial widths, field amplitudes, and transmission coefficients, can be calculated. These results also enable solving inverse problems, namely, to find (with some accuracy) the absorption rate of the medium and the positions of the effective cavities, using the measured transmission and reflection coefficients as the input data. The analytical results deduced from quantum-mechanical analogy are in close agreement with the results of direct numerical simulations.

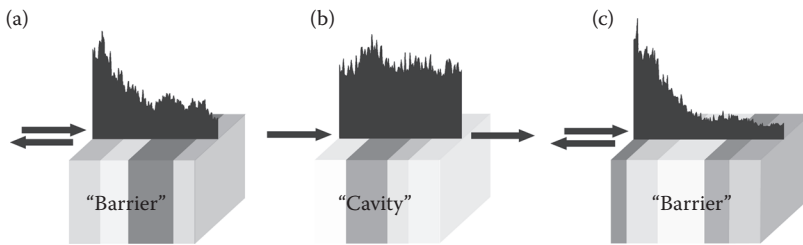


**FIGURE 2.4.4**

(See color insert.) Amplitude of the field as a function of the coordinate inside the whole sample, in the (a), (b), and (c) parts taken as a separate sample each. (Reprinted with permission from K. Bliokh et al., *Rev. Mod. Phys.* **80**, 1201, 2008. Copyright 2008 by the American Physical Society.)

The idea of this mapping was inspired by the well-pronounced similarity between [Figures 2.4.3](#) and 2.4.4 obtained for a random stack of layers, and the corresponding dependencies calculated for a regular potential well bounded at both sides by two potential barriers (e.g., see Ref. 33). Although the physics of the propagation in each system is totally different (interference of the multiply-scattered random fields in a randomly layered medium, and tunneling through a regular two-humped potential), the affinity between them stands out. Indeed, in both cases, the transmission coefficients are exponentially small for most of the frequencies (energies) and have well-pronounced resonant maxima (sometimes of the order of unity) at discrete points corresponding to the eigen levels of each system. The energy at resonant frequencies is localized, and the transmission depends drastically on the position of the area of localization.

Figure 2.4.4 presents the transparencies of three segments of the sample cut in accordance with the central curve (resonant wave) in [Figure 2.4.3](#) and separately illuminated by the same resonant (for the whole sample) wave. It is seen that at the resonant frequency, the middle part where the energy is concentrated is almost transparent, whereas the side sections are practically opaque. This qualitatively corresponds to what happens to quantum particles in a potential well. Moreover, even quantitatively, the intensity distributions presented in [Figure 2.4.3](#) and the corresponding values of the transmission coefficients compare favorably with those calculated quantum-mechanically by solving [Equation 2.4.1](#), with the random function  $\delta\epsilon(x)$  being replaced by a regular potential profile with properly chosen parameters.

For any (not too high) energy, the transmission coefficient of a two-humped potential profile (potential well) can be calculated in the Wentzel–Kramers–Brillouin (WKB) approximation,<sup>33</sup> which yields expressions independent of the “fine structure” of the profile and uniquely determined by the size of the well and by the tunneling transparencies of the bounding barriers. To use these formulae for the quantitative description of the wave transmission through a random sample, it is necessary to express the parameters of the effective potential through the parameters of the disordered system in hand. For an ensemble of 1D random realizations, those parameters are the length  $L$  of the samples and the (self-averaging) localization length  $l_{\text{loc}}$  ([Equation 2.4.6](#)). Note that in the localized regime,  $L \gg l_{\text{loc}} \gg \lambda$ . This inequality justifies the validity of the WKB approximation. To estimate the length of the effective well, we note that the appearance of a transparent segment (effective well) inside a random sample is the result of a very specific (and therefore low-probable) combination of phases of the multiply-scattered fields. Obviously, the longer such segment the less the probability of its occurrence. On the

other hand, the typical scale in the localized regime is  $l_{\text{loc}}$ . Hence, the minimal and thus the most probable size of the effective well,  $l_{\text{res}}$ , is of the order of the localization length, which we assume (as a result of self-averaging) to be the same in all realizations. Under this assumption, different values of the resonant transmission coefficients and different intensities can be reproduced by variations of the location of the well in the corresponding quantum-mechanical formulae.

If the center of the transparent segment of a resonant realization is shifted a distance  $d$  from the center of the sample, the lengths of the nontransparent parts of the resonant realizations become

$$L_{1,2} = \frac{L - l_{\text{res}}}{2} \pm d, \quad (2.4.25)$$

and the transmission coefficients of the confining barriers are

$$T_{1,2} = \exp\left(-\frac{L_{1,2}}{l_{\text{loc}}}\right). \quad (2.4.26)$$

Substituting Equations 2.4.25 and 2.4.26 into the corresponding WKB formulae, we obtain

$$T_{\text{res}}(d) = \frac{4T_1T_2}{(T_1 + T_2)^2} = \frac{4}{[\exp(d/l_{\text{loc}}) + \exp(-d/l_{\text{loc}})]^2}, \quad (2.4.27)$$

$$|A_{\text{res}}(d)|^2 = \frac{8T_1}{(T_1 + T_2)^2} = \frac{8\exp(L/l_{\text{loc}} - 1 - d/l_{\text{loc}})}{[\exp(d/l_{\text{loc}}) + \exp(-d/l_{\text{loc}})]^2}, \quad (2.4.28)$$

where  $T_{\text{res}}(d)$  and  $A_{\text{res}}(d)$  are, respectively, the transmission coefficient and the peak amplitude of the field pumped into the cavity located at a point  $d$  by an incident resonant monochromatic wave of unit amplitude. Note that  $|A_{\text{res}}|^2$  is asymmetric with respect to  $T_1$  and  $T_2$ , which means that the intensity induced in an effective cavity by the resonant incident wave depends on the direction of incidence.<sup>34</sup> The width of high ( $T_{\text{res}} \sim 1$ ) resonances in a long sample is exponentially small:

$$\delta k_{\text{res}} \sim \frac{1}{l_{\text{loc}}} \exp\left(-\frac{L}{l_{\text{loc}}}\right). \quad (2.4.29)$$

Equation 2.4.27 shows that the transmission coefficient of a disordered sample at a resonance is independent of the length of the sample and is governed exclusively by the location of the effective cavity. This rather counterintuitive result is totally different from that for the typical (nonresonant) transmission, which decays exponentially with the increase of the length  $L$ .

From Equation 2.4.28 it follows that the amplitudes of the centrally located ( $d \ll l_{\text{loc}}$ ) strong resonances are an exponentially increasing functions of the length of the sample:

$$|A|^2 \approx 2\exp\left(\frac{L}{l_{\text{loc}}}\right) \gg 1. \quad (2.4.30)$$

Whereas the transmission is maximal when the effective cavity is located precisely in the middle of the sample,  $T_{\text{res}}(d=0) = 1$ , the largest amplitude can be pumped in a resonator shifted from the center toward the input by the distance

$$d_A = -0.27l_{\text{loc}}, \quad (2.4.31)$$

which is independent of the length of the sample.

It should be emphasized that in a disordered sample, for each resonant frequency,  $\omega_{\text{res}}$ , there exists its own “strange resonator,” which (unlike regular potential wells) is transparent only for this particular  $\omega_{\text{res}}$ . These resonators are located at different random points; therefore, it should be remembered that the coordinate  $d$  in Equations 2.4.25 through 2.4.28 is frequency-dependent:  $d = d(\omega_{\text{res}})$ . The structure of the effective cavities is described below.

To test the ability of the above-introduced deterministic model to describe quantitatively the resonances in randomly layered samples, extensive numerical experiments were carried out. The comparison of the results of direct numerical simulations with those given by Equations 2.4.27 through 2.4.31 demonstrates that the seemingly rough analogy based on just one fitting parameter (localization length) performs surprisingly well.<sup>31</sup> For example, not only the coordinate of the effective cavity with the highest resonant amplitude is independent of the total length of the sample and proportional to  $l_{\text{loc}}$ , as predicted by Equation 2.4.31, but also the coefficient in Equation 2.4.31 coincides with that obtained in numerical simulations with an accuracy  $\sim 10\%$ .

To provide an adequate description of the resonances in real dielectric structures, the absorption should be incorporated in the model. Although in quantum-mechanical problems losses are rather uncommon, the absorption of light in a dielectric medium can be taken into account by formally adding to the corresponding effective potential a negative imaginary part proportional to the imaginary part of the permittivity. If the spatial decrement of the wave energy due to loss,  $\Gamma = 1/l_a \sim \text{Im}\epsilon_0$ , is small compared to the inverse localization length,  $l_a \gg l_{\text{loc}}$ , calculations of the resonant transmittance and intensity yield<sup>35</sup> (compare with Equations 2.4.27 and 2.4.28):

$$T_{\text{res}}(d) = \frac{4T_1T_2}{(\Gamma l_{\text{res}}\sqrt{\text{Re}\epsilon_0} + T_1 + T_2)^2}, \quad (2.4.32)$$

$$|A_{\text{res}}(d)|^2 = \frac{2T_{\text{res}}}{T_2}. \quad (2.4.33)$$

The connection between the resonant reflection and transmission coefficients follows from the energy conservation law and in, a case of small losses, takes the form

$$R_{\text{res}} = 1 - T_{\text{res}} - \Gamma l_{\text{res}} |A_{\text{res}}|^2 \sqrt{\text{Re}\epsilon_0}, \quad (2.4.34)$$

where the last term is due to absorption in the medium. The width of the resonant peak in the reflection is determined by the absorption in the medium and by the transmittance of the effective walls that form the effective wells, and is equal to

$$\delta k_{\text{res}} = \Gamma + \frac{T_1 + T_2}{l_{\text{res}}\sqrt{\text{Re}\epsilon_0}}. \quad (2.4.35)$$

When the parameter

$$b = 2\Gamma l_{\text{res}} \sqrt{\text{Re} \epsilon_0} \exp\left(\frac{L}{2l_{\text{loc}}}\right) \gg 1, \quad (2.4.36)$$

even small absorption ( $l_a \gg l_{\text{loc}}$  or  $l_a \gg L$ ), which practically does not affect the typical transmission, suppresses dramatically both the reflected and transmitted fluxes at resonances. Interestingly, the resonant reflection coefficient, Equation 2.4.34, is a nonmonotonic function of the dissipation rate  $\Gamma$ , and turns to zero when  $b = -2\sinh(d/l_{\text{loc}})$ . This effect is known in optics and microwave electronics as critical coupling.<sup>36</sup> As no energy is reflected from the sample at critical coupling, it corresponds to the resonance with the highest intensity.

#### 2.4.4.2 How Is an Effective Cavity Built Up?

The model presented above gives a more penetrating insight into the mechanism of formation of localized modes and allows an explanation of how and why the characteristics of a resonance (Q-factor, transmission coefficient, linewidth, etc.) depend on the parameters of the effective cavity (location, size, and absorption rate) associated with it. It is now clear that the resonant transmission through a random sample takes place at a frequency  $\omega_{\text{res}}$  if around some (random) point inside this sample there exists an area of length  $l_{\text{res}} \gtrsim l_{\text{loc}}$  which is transparent for this frequency.

Here another question arises: why do effective resonant cavities exist in 1D disordered samples? In other words, why are different segments of a random configuration transparent or opaque for the wave with a given wave number  $k$ ? To answer this question recall that in the case of weak scattering, the so-called resonance reflection takes place; that is, the reflection coefficient of an adequately long segment  $[x - a, x + a]$  of a random medium is proportional to the amplitude of the  $2k$ -harmonic in the power spectrum,  $\tilde{\epsilon}(2k, x)$ , of its dielectric constant  $\epsilon(x)$ .<sup>37</sup> This amplitude can be calculated as

$$\tilde{\epsilon}(2k, x) = \int_{x-a}^{x+a} \epsilon(y) e^{-i2ky} dy. \quad (2.4.37)$$

This expression is known as a window Fourier transformation with a rectangular window function. To investigate the structure of a resonant configuration, we first determined the resonant wave numbers for which the transparency  $T(k)$  of this configuration exceeded, for example, 0.5. For each of those waves, the spatial distributions of the amplitude and of the corresponding local power spectrum (2.4.37) were juxtaposed. An example is shown in [Figure 2.4.5](#). One can see that in the areas where the field is localized, the function  $\tilde{\epsilon}(2k, x)$  is strongly suppressed, whereas in the nontransparent parts it has well-pronounced maxima. Therefore, the resonant cavity for a frequency  $\omega_{\text{res}}$  arises in the area of a disordered sample where, accidentally, the harmonic with wave number  $q_{\text{res}} = 2k_{\text{res}}$  in the power spectrum of the (random) permittivity has small amplitude.

This result is of profound importance for the correct understanding of the resonant transparency of 1D random systems. It has been commonly accepted that, in accordance with the celebrated formula (2.4.8), high (not “typical,” exponentially small) transparency at a given frequency requires the suppression of the corresponding spatial spectral component *in the whole sample*. A fundamentally new outcome of the above consideration is that for arising of a localized eigenmode, which provides resonant transmission, it suffices for the  $2k_{\text{res}}$ -harmonic to be suppressed in a *much smaller area of size*  $l_{\text{res}} \gtrsim l_{\text{loc}}$ .

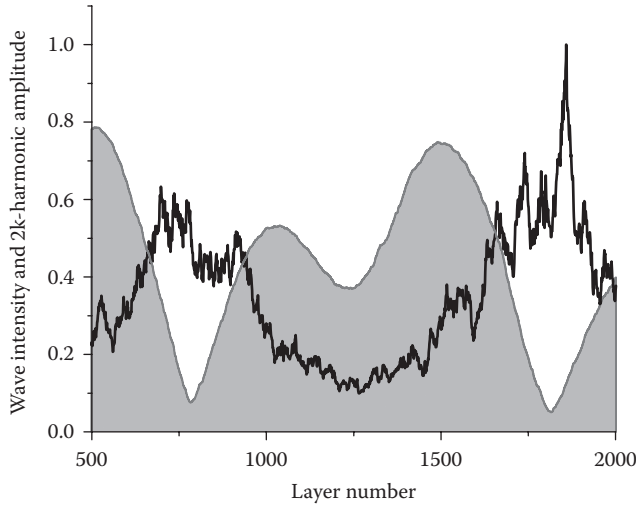


**FIGURE 2.4.5**

Normalized wave (black line) and  $2k$ -harmonic (gray area) amplitudes as functions of the coordinate (layer number).

Obviously, the probability of such a random event is exponentially (with respect to  $L/l_{\text{res}} \gg 1$ ) larger than that of the same to occur simultaneously in the whole random configuration. This not only explains the observed high spectral density of the eigenstate (2.4.3) but also provides a background for harnessing disordered 1D systems in designing tunable light-tailoring devices (see Section 2.4.7).

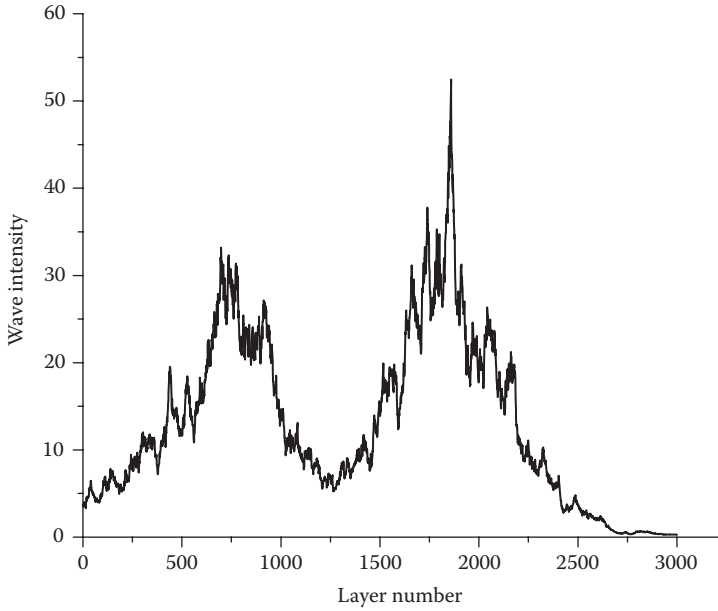
### 2.4.4.3 Coupling and Level Repulsion

An adequately long, disordered 1D sample can contain several isolated regions where the spectral harmonics with wave numbers close to  $q_{\text{res}}$  are suppressed. The spatial overlap of the wave functions localized in such regions couples these modes and leads to the formation of the so-called necklace states, which have been predicted theoretically in the studies by Lifshits and Kirpichenkov<sup>38</sup> and by Pendry<sup>11</sup> and observed and studied experimentally in Refs. 9 and 39. These states have broadened spectral lines<sup>7</sup> and contribute substantially to the overall transmission in localized regime. An example of a necklace state is shown in [Figure 2.4.6](#).

Necklace states can be easily incorporated in the modeling scheme as two or more potential wells coupled by the evanescent fields that tunnel through barriers separating the wells.<sup>9,32</sup> The temporal dynamics of the field in such a chain of coupled resonators is described by a system of oscillator equations with an external force, damping, and coupling coefficient, which account for the incident wave, the finite  $Q$ -factors, and the spatial overlap of the modes, respectively. In the simplest case of two cavities with coordinates  $d_1$  and  $d_2$ , the equations that provided an effective description of coupled modes can be written as:<sup>32</sup>

$$\frac{d^2\psi_1}{d\tau^2} + Q_1^{-1} \frac{d\psi_1}{d\tau} + (1 - \Delta_1)^2 \psi_1 = q\psi_2 + f, \quad (2.4.38)$$

$$\frac{d^2\psi_2}{d\tau^2} + Q_2^{-1} \frac{d\psi_2}{d\tau} + (1 - \Delta_2)^2 \psi_2 = q\psi_1. \quad (2.4.39)$$

**FIGURE 2.4.6**

Necklace state. Normalized wave intensity as a function of the coordinate (layer number).

Here  $\psi_i(\tau)$  is the field in the  $i$ th effective resonator,  $\tau = \omega_0 t$  is the dimensionless time ( $\omega_0$  is a characteristic central frequency of the problem), and  $1 - \Delta_i$  ( $|\Delta_i| \ll 1$ ) is the dimensionless (in units of  $\omega_0$ ) eigenfrequency of the  $i$ th resonator. The effective external force  $f$  is

$$f = \psi_0 \exp\left(\frac{-d_1}{l_{\text{loc}}}\right) e^{-i\nu\tau}, \quad (2.4.40)$$

where  $\psi_0$  and  $\nu$ , ( $|\nu - 1| \ll 1$ ), are the amplitude and the frequency of the external field, exciting the first (close to the input) resonator. The coupling coefficient  $q \ll 1$  of two cavities, which is due to the spatial overlap of modes, is equal to

$$q = \exp\left(\frac{-d}{l_{\text{loc}}}\right) \quad (2.4.41)$$

with  $d$  being the distance between the effective cavities.

The  $Q$ -factors describing the losses of energy in the  $i$ th resonator are:<sup>40</sup>

$$Q_i^{-1} = \Gamma_i + \frac{v_g T_i}{2l_i \omega_0} \ll 1, \quad (2.4.42)$$

where  $\Gamma_i$  is the dissipation rate in the  $i$ th resonator,  $v_g$  is the wave group velocity inside the resonator, and  $l_i$  is the cavity length. The last term in Equation 2.4.42 accounts for the

leakage of the energy from the system; therefore, analogously to Equation 2.4.26, the transmission coefficients  $T_{1,2}$  are given by<sup>32</sup>

$$\begin{aligned} T_1 &= \exp\left(\frac{-d_1}{l_{\text{loc}}}\right), \\ T_2 &= \exp\left[-\left(\frac{L-d_2}{l_{\text{loc}}}\right)\right]. \end{aligned} \quad (2.4.43)$$

Substitution  $\psi_i = A_i \exp(-i\nu\tau)$  reduces Equations 2.4.38 and 2.4.39 to a couple of algebraic equations, from which the eigenfrequencies of two complex independent eigenmodes of the system can be found:

$$\nu^\pm = 1 - \frac{\Delta_1 + \Delta_2}{2} - i \frac{Q^{-1}}{2} \pm \frac{1}{2} \sqrt{(\Delta_1 - \Delta_2)^2 + q^2}. \quad (2.4.44)$$

We have assumed here that  $Q_1 = Q_2 = Q$ . Depending on the parameters, Equation 2.4.44 describes either level anticrossing (level repulsion) or the coupling of isolated resonators to form collective eigenmodes. The anticrossing takes place when the eigenfrequencies of two cavities come close and are transformed into double-peaked, more extended modes. The gap between eigenfrequencies is equal to

$$G_e = \sqrt{(\Delta_1 - \Delta_2)^2 + q^2}, \quad (2.4.45)$$

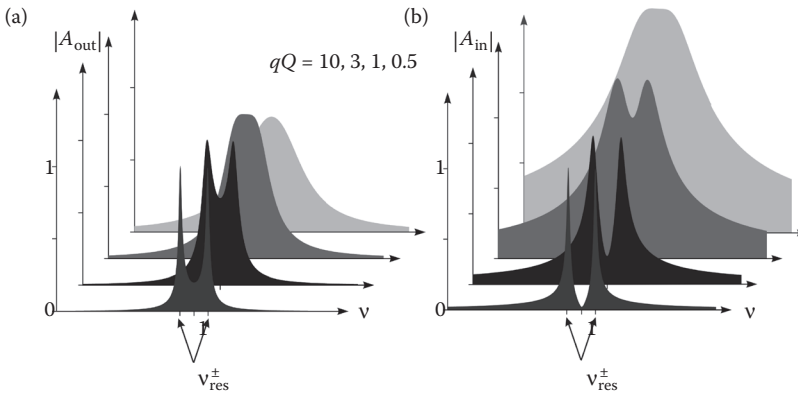
and is minimal at the resonance,  $\Delta_1 = \Delta_2$ . Note that the level repulsion of modes, that is generally agreed to be an inherent feature of diffusion, arises here in the regime of strong localization. Away from resonance,  $|\Delta_1 - \Delta_2| \gg q$ , the eigenmodes tend to the modes of isolated resonators. The shapes of the modes are exchanged when passing through the resonance; that is,  $+$  ( $-$ ) eigenmodes correspond to the first (second) resonator at  $\Delta_1 \ll \Delta_2$ , and to the second (first) resonator when  $\Delta_1 \gg \Delta_2$ .

The frequency ( $\nu$ ) dependences of the amplitudes  $A_1$  and  $A_2$  of the oscillations induced in the cavities by incident monochromatic waves are determined by the ratio between the coupling coefficient  $q$  and losses  $Q^{-1}$ . Both amplitudes are at maximum at two frequencies

$$\nu_{\text{max}}^\pm = 1 - \frac{\Delta_1 + \Delta_2}{2} \pm \frac{1}{2} \sqrt{q^2 - Q^{-2}}. \quad (2.4.46)$$

There are two different regimes of the excitation of coupled resonators, depending on the value of the  $qQ$  factor, as shown in [Figure 2.4.7](#) for the case of identical ( $\Delta_1 = \Delta_2 = 0$ ) cavities.<sup>32</sup> When losses are small, so that the condition  $qQ > 1$  holds, there are two collective anticrossing resonant modes with the frequency gap  $G_A = \sqrt{q^2 - Q^{-2}}$  and equal field amplitudes in both resonators. As  $qQ$  decreases, the resonant peaks in the spectra are located near each other and meet when  $qQ = 1$ . In the regime  $qQ < 1$ , there is one peak at  $\nu = 1$ .

The parameter  $qQ$  that appears in the model has a simple physical meaning: it determines whether the two resonators should be considered as essentially coupled or isolated. When  $Q^{-1} \ll q$ , the losses are negligible and the field characteristics are

**FIGURE 2.4.7**

(See color insert.) Near-resonant transmission of an incident wave through two coupled open resonators at different values of  $qQ$ . The normalized (i.e., multiplied by the factor  $2Q^{-1}$ ) absolute values of the field amplitudes in two resonators,  $|A_{\text{out}}|$  (a) and  $|A_{\text{in}}|$  (b), are shown. (Reprinted with permission from K. Bliokh et al., *Rev. Mod. Phys.* **80**, 1201, 2008. Copyright 2008 by the American Physical Society.)

essentially determined by the coupling. Remarkably, in this case the field intensity in the first (incoming) resonator is negligible at  $v = 1$ , and almost all the energy is concentrated in the second resonator:  $A_2 \gg A_1$ . On the contrary, when the losses prevail over the coupling,  $Q^{-1} \gg q$ , the incident wave only excites the first resonator, and the energy is concentrated mostly in it:  $A_1 \gg A_2$ .

#### 2.4.4.4 Bistability of Anderson Localized States in Nonlinear Random Media

A combination of disorder and nonlinearity offers a multitude of striking physical phenomena, some of which still remain enigmatic and call for further investigation. In particular, nonlinear interactions between electromagnetic radiation and disorder influences the interference of the multiply-scattered waves and can affect localization in rather unusual ways. This area has long been the subject of keen scientific interest that has quickened recently, mostly as a result of the creation of high-power lasers and of the latest advancement in studies of Bose–Einstein condensates. Although publications on the transport and localization in nonlinear random media are numerous, the overwhelming majority of the analytical results have a common shortcoming: they are related to ensemble-averaged characteristics, which are of a little use when individual localized states are concerned. A breakthrough in the theoretical study of the disorder-induced resonances has been made possible with the above-presented quantum-mechanical deterministic model, in which the nonlinearity was incorporated. Surprisingly, this rather simple approach not only offered a clearer insight into the physics of the resonances in nonlinear random media but also performed well in their quantitative description.<sup>13</sup>

According to the model, the transmittance spectrum  $T(k)$  in the vicinity of a resonant wavelength,  $|k - k_{\text{res}}| \ll k_{\text{res}}$  is given by the Lorentzian dependence

$$T(k) = \frac{I_{\text{out}}}{I_{\text{in}}} = \frac{T_{\text{res}}}{1 + [2Q(k/k_{\text{res}} - 1)]^2}, \quad (2.4.47)$$

where  $I_{\text{in}}$  and  $I_{\text{out}}$  are the intensities of the incident and outgoing waves, respectively. The resonant transmission coefficient  $T_{\text{res}} = T(d)$  is given by Equation 2.4.32, where  $d = d(k_{\text{res}})$ .

Obviously, the nonlinearity becomes most noticeable at the points where the resonances are located and the intensity is maximal,  $I = I_{\text{res}}$ . It changes the effective refractive index of the medium leading to the intensity-dependent shift of the resonant wave number:  $k_{\text{res}} \rightarrow \tilde{k}_{\text{res}}(I_{\text{res}})$  (Figure 2.4.8).

As the values of  $I_{\text{res}}$  and  $I_{\text{out}}$  are unambiguously connected, the resonant wave number is a function of the output intensity, and Equation 2.4.47 establishes a relation between the input and output wave intensities, which in the case of weak Kerr-type nonlinearity is cubic with respect to  $I_{\text{out}}$ .<sup>13</sup> It has a universal form typical of nonlinear resonators with optical bistability.<sup>41</sup> The ultimate dependence  $I_{\text{out}}(I_{\text{in}})$  is of the S-type, and, in some range of parameters, the stationary transmission spectrum  $T(k)$  is a three-valued function. Typically, one of the solutions is unstable, whereas the other two form a hysteresis loop in the  $I_{\text{out}}(I_{\text{in}})$  dependence.<sup>13</sup> Figure 2.4.8 shows nonlinear deformations of the resonant transmission spectra  $T(k)$ , which at large values of the parameter  $\chi I_{\text{in}}$  ( $\chi$  is the Kerr coefficient) exhibit transitions to bistability. The analytical dependence  $T(k)$ , derived from Equation 2.4.47, with parameters found from the numerical experiments, are in excellent agreement with the direct numerical simulations.

The adequacy of the model has also been substantiated by numerical modeling in time domain. In these simulations, the transitional oscillations and reshaping of the transmitted pulse that typically accompany switching between two regimes of transmission in deterministic bistable nonlinear structures<sup>42</sup> have been found in disordered nonlinear samples. Nonreciprocity (diode-like unidirectional propagation) of resonant tunneling

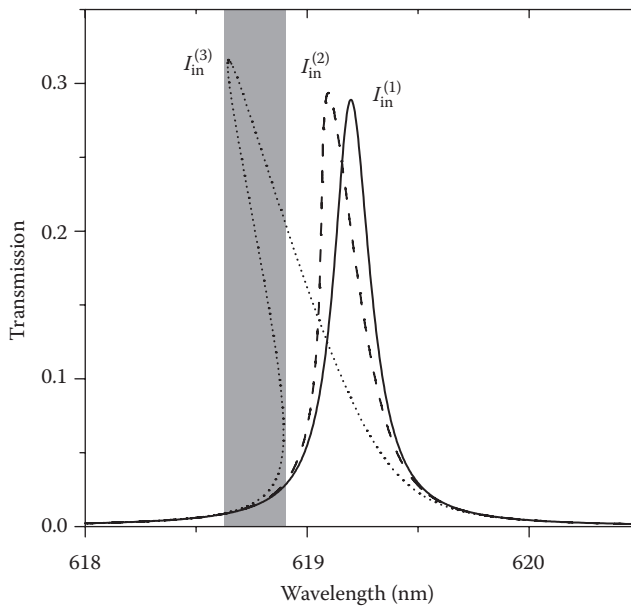


**FIGURE 2.4.8**

Nonlinear deformations of the transmission spectrum of the resonance at different intensities  $I_{\text{in}}^{(1)} < I_{\text{in}}^{(2)} < I_{\text{in}}^{(3)}$  of the incident wave. The light-gray stripe indicates the three-valued region. Only the lower and upper branches of the transmission spectrum are stable. (Reprinted with permission from I. Shadrivov et al., Phys. Rev. Lett. **104**, 123902, 2010. Copyright 2010 by the American Physical Society.)

through a nonlinear random structure that stems from the intrinsic asymmetry of disorder has also been observed.

### 2.4.5 Experimental Studies of Resonances

Comprehensive experimental studies of localized states and disorder-induced resonances were carried out in the microwave frequency range ( $14 \text{ GHz} \leq f \leq 20 \text{ GHz}$ ).<sup>9,35</sup> A long metallic single-mode (at these frequencies) waveguide filled with randomly arranged, weakly absorbing dielectric slabs were used as 1D disordered system. The experimental setup allowed measurements of the complex transmission and reflection amplitudes and the complex field inside the waveguide for different random configurations. Figure 2.4.9 depicts the intensity  $I(x, f) \equiv |A(x, f)|^2$  generated inside a sample by an incident monochromatic wave with frequency  $f$ , as a function of coordinate  $x$  and frequency  $f$ .<sup>35</sup> Although the “fine structure” of the field changes dramatically from sample to sample, the general features intrinsic in all 1D disordered systems are clearly recognized in the results of a single measurement presented, as an example, in Figure 2.4.9. Localized states (resonances) excited by the incident wave are clearly seen in Figure 2.4.9. When  $b \gg 1$  (Equation 2.4.36), the highest of them are located in the left (close to the input) part of the sample. The transmitted signal is suppressed by losses below the experimental noise and is indiscernible in Figure 2.4.9 even at resonant frequencies. At the same time, the resonances manifest themselves (and can be easily detected) by sharp dips in the frequency dependence of the reflection coefficient (see Figure 2.4.10). Moreover, at different values of  $b$  (i.e., of  $\Gamma$ ) localized eigenstates are excited and detectable in reflection in different regions of the system, thus providing a possibility for scanning the sample through variations of losses. This means that dissipation, which usually impairs the excitation and observation of resonances in 1D random samples improves essentially the “observability” of the localized states.

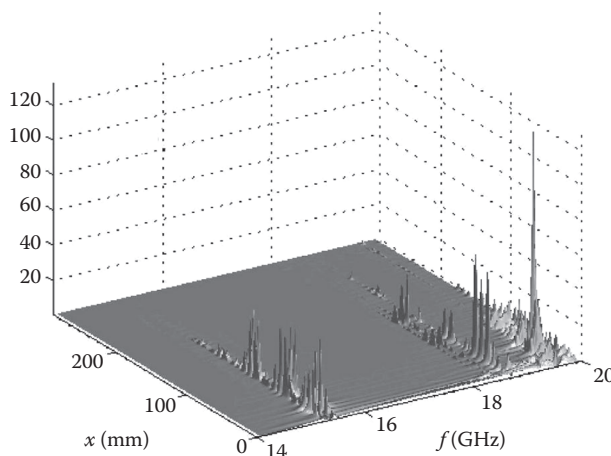


**FIGURE 2.4.9**

Intensity versus frequency and position inside the sample. (Reprinted with permission from K. Bliokh et al., *Phys. Rev. Lett.* **97**, 2439094, 2006. Copyright 2006 by the American Physical Society.)

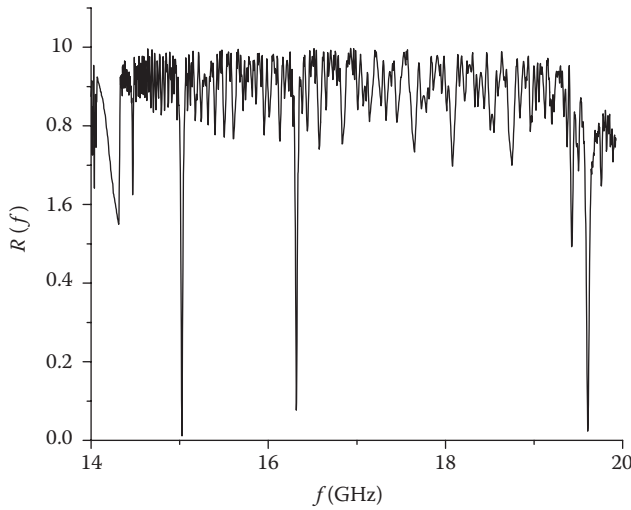


**FIGURE 2.4.10**

Spectrum of reflection for [Figure 2.4.9](#). (Reprinted with permission from K. Bliokh et al., *Phys. Rev. Lett.* **97**, 2439094, 2006. Copyright 2006 by the American Physical Society.)

In the study by Bliokh et al.,<sup>9</sup> the same setup was used to explore experimentally the dynamics of formation of the necklace states and to study their spectral and transport properties. Measurements were made in a sequence of configurations in which the spacing between two randomly located scatterers could change steps in a controlled way. The position at which the air gap was introduced was chosen to correspond to the peak of a single Anderson localized mode of the unperturbed random sample. This allowed to manipulate the frequency of the selected mode in a manner similar to the tuning of a defect state through a band gap in a periodic structure. In doing so, the mode frequency shifted and crossed the frequencies of other localized states, which made it possible to study the coupling of modes. Changing the air spacing at points where other states have been localized, allowed to couple several localized modes, thereby creating necklace states extended throughout the sample. The spectral positions of the localized states as functions of the air gap introduced into the sample are plotted in [Figure 2.4.11](#). The frequencies of modes either cross or anticross, in reasonable compliance with Equation 2.4.44. Direct measurements of the electromagnetic field inside the samples have revealed that in the case of anticrossing (regions 1,2,4,5 in [Figure 2.4.11](#)), the coupling within the sample was accompanied by the theoretically predicted exchange of shapes. In contrast, when modes crossed (region 3 in [Figure 2.4.11](#)) they did not exchange shapes and remained practically independent of each other. When the frequencies of the modes were closest, the two localized states coupled into double-peaked modes signifying the formation of quasi-extended necklace states.

The minimum frequency differences were calculated for the interacting pairs 1,2,4,5 in [Figure 2.4.11](#), as  $G_A = \sqrt{q^2 - Q^2}$  with  $q$  and  $Q$  found from Equations 2.4.41 and 2.4.42, and then compared to the measured values of the gap. A comparison of the measured and calculated data is presented in [Figure 2.4.12](#) for the following parameters of the system:<sup>9</sup>  $f_0 = \omega_0/2\pi = 15.5$  GHz,  $l_{\text{loc}} = 12$  mm,  $\omega_0\Gamma = 7 \times 10^7 \text{s}^{-1}$ , and  $v_g = c/2.4$ . Good agreement exists between the experiment and the model.

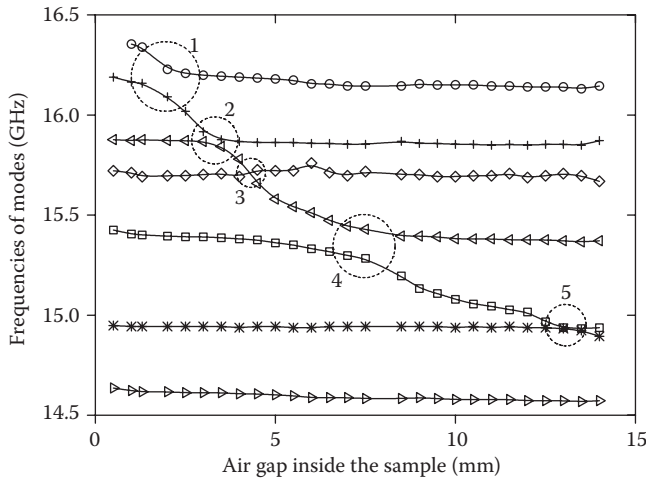


**FIGURE 2.4.11**

Resonant frequencies of excited localized modes versus the driving parameter—the air gap inside the sample. Five pair-interaction regions are circled. (Reprinted with permission from K. Bliokh et al., *Phys. Rev. Lett.* **101**, 133901, 2008. Copyright 2008 by the American Physical Society.)

Anderson localization of millimeter electromagnetic waves (75–110 GHz) has been studied experimentally,<sup>12</sup> utilizing 100-layer dielectric stacks of randomly shuffled quartz and Teflon wafers. Exponentially small transmission at typical frequencies, resonant transmission at eigenfrequencies, and enhanced absorption have been observed. Slow light and superluminal group velocities, which in contrast to photonic crystals were not associated with any periodicity in the system, have also been discovered.

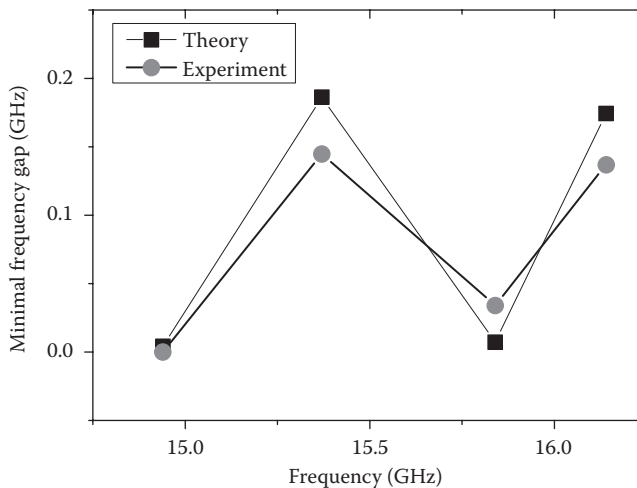


**FIGURE 2.4.12**

Experimentally measured and theoretically calculated minimal frequency gaps  $G_A = \sqrt{q^2 - Q^2}$  for pairs of interacting modes 1,2,4,5 presented in Figure 2.4.11. (Reprinted with permission from K. Bliokh et al., *Phys. Rev. Lett.* **101**, 133901, 2008. Copyright 2008 by the American Physical Society.)

### 2.4.5.1 Inverse Scattering Problems and Remote Sensing of Disordered Samples

Microwave experiments<sup>9,12,35</sup> made it possible to test immediately the validity of the model introduced in Section 2.4.4. Theoretical predictions based on the model have been checked against the results of measurements carried out at a large number of random configurations and in a wide range of parameters. It turned out that Equations 2.4.23 and 2.4.32 through 2.4.35 not only provided a new insight into the physics of the experimentally observed features presented in the previous subsection but also were in a good quantitative agreement with the measured data. This was made possible using these equations as a basis for formulation and solving a classical wave inverse problem: retrieval of internal characteristics of a medium of propagation from parameters of the external fields. In practice, an algorithm of remote sensing of random samples have been developed, which has enabled nonintrusive detection and monitoring of the disorder-induced resonances and determination of the absorption and localization lengths by measuring the reflected and transmitted fields. The algorithm is very simple. Indeed, Equations 2.4.23 and 2.4.32 through 2.4.35 can be treated as four algebraic equations for four unknowns, and by solving them one can find the location,  $d$ , and the size,  $l_{\text{res}}$ , of an effective cavity for each resonant frequency, and the localization and absorption lengths of the sample. Then, the intensity,  $A_{\text{res}}$ , pumped in a cavity by the incident wave can be calculated by Equation 2.4.30.

In such a manner, these parameters had been retrieved in Ref. 12 for many disordered configurations, using the directly measured values of  $T_{\text{res}}$ ,  $R_{\text{res}}$ ,  $\delta f = c\delta k_{\text{res}}$ , and  $l_{\text{loc}}$ . An example is presented in Table 2.4.1. Shown in columns 2, 3, and 4 are  $1 - R_{\text{res}}$ ,  $T_{\text{res}}$ , and  $\delta f$ , respectively, measured for the resonances indicated in column 1. The loss tangent,  $\tan(\alpha) = \Gamma c / f \sqrt{\text{Re}\epsilon_0}$ , is given in column 6. The value of the loss tangent averaged over the five resonances equals  $8.35 \times 10^{-4}$ . The genuine weighted loss tangent for the disordered quartz/Teflon system was  $5.2 \times 10^{-4}$ , so that the measured and retrieved values of the absorption agreed to within the accuracy of the experiment. Similar experiments in the centimeter-wavelength range<sup>35</sup> also yielded retrieved data consistent with the true values.

The remote sensing procedure can be also applied for monitoring nonlinear disordered samples. In this instance,  $T_{\text{res}}$ ,  $k_{\text{res}}$ , and  $Q$  are determined from the transmission spectrum in the linear regime as it was described above, and the additional external parameter of the medium—Kerr coefficient—is retrieved from the measured shift of the transmission spectral line when the intensity changes. This enables one to obtain the whole dependence  $I_{\text{out}}(I_{\text{in}}, k)$  for any given resonance performing external measurements of  $T(k)$  at only two different intensities of the incident wave.

**TABLE 2.4.1**

Measured and Calculated Parameters Associated with Five Resonances

Frequency (GHz)	$1 - R_{\text{res}}$	$T_{\text{res}}$	$\delta f$ (GHz)	$G/\sqrt{\epsilon} \cdot 10^2$	$\tan \alpha \cdot 10^4$
$f_1 = 83.5$	0.978	0.75	0.40	0.83	4.77
$f_2 = 92.0$	0.998	0.33	0.39	2.6	13.45
$f_3 = 105.7$	0.993	0.31	0.34	2.25	10.14
$f_4 = 101.8$	0.87	0.18	0.25	1.33	6.22
$f_5 = 99.8$	0.77	0.30	0.45	1.5	7.16

Source: Reprinted with permission from J. Scales et al., Phys. Rev. B **76**, 085118, 2007. Copyright 2007 by the American Physical Society.

Note: The localization length is 1 cm (obtained from the nonresonant transmission coefficient).

---

## 2.4.6 Anderson Localization in Exotic Materials

### 2.4.6.1 Suppression of Anderson Localization in Disordered Metamaterials

The theoretical study of any newly discovered physical phenomenon or laboratory-created material always starts from a simplified, ideal model, which makes it possible to understand the underlying principles and to explain the basic features observed in the pioneering experiments. More in-depth investigations call for more realistic models. Sooner or later, in particular when it comes to applications, taking account of disorder becomes necessary. Such is indeed the case in the current status of research on metamaterials and graphene.

Unusual physical properties of metamaterials open up unique possibilities for numerous applications in modern optics and microelectronics. As all real metamaterials are always disordered (mostly as a result of inevitable fabrication errors), the investigation of the effects of random scattering on their transport properties is not only a fundamental academic problem but is also of significant practical importance.

The analytical and numerical analyses based on the transfer matrix method presented in Section 2.4.3 show that in stratified media with alternating layers of right- and left-handed materials (mixed stacks), the localization properties differ dramatically from those exhibited by conventional disordered materials. In particular, at long wavelengths, the localization length of mixed stacks with random refractive indices and nonfluctuating thicknesses is proportional to the sixth power of the wavelength, the result that has been neither predicted nor observed in conventional 1D random media.<sup>14,15</sup> It means that left-handed metamaterials can substantially suppress Anderson localization in 1D disordered systems. The suppression reveals itself also in the vanishing of the disorder-induced resonances when left-handed layers are added to a random stack of normal dielectrics. This is attributable to the lack of phase accumulation over a mixed sample, due to the cancellation of the phase across alternating left- and right-handed layers. When both refractive index and thickness of the layers constituting a mixed stack fluctuate the transmission length in the long-wave range of the localized regime exhibits the well-known quadratic power wavelength dependence with different coefficients of proportionality for mixed and homogeneous (only metalayers) random stacks. However, the transmission length of a mixed stack differs from the reciprocal of the Lyapunov exponent of the corresponding infinite stack, presenting a unique example of a 1D disordered system, in which the localization and transmission lengths are different. In contrast to normal disordered materials, the characteristic ballistic and localization lengths of mixed stacks are also different, at least in the weak scattering limit. The crossover region from localization to the ballistic regime is relatively narrow for both mixed and homogeneous stacks.

Polarization effects have been considered in Ref. 36. It is shown that the transport length strongly depends on the angle of incidence for both vertical ( $p$ ) and horizontal ( $s$ ) polarizations of the incident wave. In particular, when the angle of incidence exceeds a critical angle, an additional exponential decay arises due to the internal reflection from the individual layers. In mixed stacks with only refractive-index disorder,  $p$ -polarized waves are strongly localized, whereas for the  $s$ -polarization the localization is substantially suppressed at all angles of incidence. The Brewster anomaly angle depends on both the polarization and the nature of disorder, that is, disorder in either the permittivity or the permeability. For incidence at the Brewster angle, localization is suppressed, and, in

contrast to the case of normal incidence, the localization length is proportional to the square of the variance of the fluctuations rather than to the variance itself.

The effects of absorption on 1D transport and localization have been studied both analytically and numerically.<sup>15</sup> It turns out that the crossover region is particularly sensitive to losses, so that even small absorption noticeably suppresses frequency-dependent oscillations in the transmission length. The disorder-induced resonances, which present an important signature of the localization regime, are also strongly affected (suppressed) by absorption.

The frequency dependence (dispersion) of the permittivity,  $\epsilon$ , and/or permeability,  $\mu$ , has a profound effect on Anderson localization leading to rather unusual, sometimes counter-intuitive phenomena. The most exotic behavior is observed in mixed stacks at the frequencies, at which  $\epsilon$  or  $\mu$  turns to zero. In this instance, the waves are delocalized for normal incidence, whereas the localization is enhanced when disorder is present in both permittivity and permeability of the layers.

#### 2.4.6.2 Transport and Localization in Disordered Graphene Superlattices

Shortly after the discovery of highly unusual physical properties of graphene, it was realized that the electron transport in this material had many common features with the propagation of light in dielectrics. In mathematical terms, under some (rather general) conditions, Dirac equations describing the charge transport in a graphene superlattice created by applying an inhomogeneous external electric potential could be reduced to Maxwell equations for the propagation of light in a dielectric medium. The role of the refractive index of this effective medium is played by the quantity  $n_{\text{eff}} = E - U$ , where  $E$  and  $U$  are, respectively, the dimensionless energy of the charge carrier and the scalar potential of the external electric field. It is easy to see that if the potential is a piecewise constant function of one coordinate, the corresponding graphene superlattice reproduces a layered dielectric structure.<sup>17</sup> In particular, a layer, in which the potential exceeds the energy of the particle,  $U > E$ , is similar to a slab with negative refractive index (metamaterial). It is because of this similarity that a junction of two regions having opposite signs of  $E - U$  (so-called p-n junction) focuses Dirac electrons in graphene in the same way as an interface between left- and right-handed dielectrics focuses electromagnetic waves.<sup>43</sup> However, the analogy is not complete: although the equations are akin, the boundary conditions are, generally, different. Comparing these conditions one can infer that in the particular case of normal incidence, the transmission of Dirac electrons through a junction is similar to the transmission of light through an interface between two media with different refractive indices but equal impedances. Such an interface is absolutely transparent to light and therefore to the Dirac electrons in graphene as well. This explains the Klein paradox (perfect transmission through a high potential barrier) in graphene systems, and leads to the surprising conclusion that Dirac electrons are delocalized in a disordered 1D graphene structure, providing a minimal nonzero overall conductivity, which cannot be destroyed by fluctuations, no matter how strong they are.<sup>44</sup> Nevertheless, many features of Anderson localization can be found in random graphene systems.<sup>17</sup> There exist a discrete random set of angles (or a discrete random set of energies for each given angle) for which the corresponding wave functions are exponentially localized. Depending on the type of unperturbed system, the disorder could either suppress or enhance the transmission. The transmission of a graphene system built of alternating p-n and n-p junctions has an anomalously narrow angular spectrum and, in some range of directions, it is practically independent of the amplitude of the fluctuations of the potential.

Disorder manifests itself in various other situations, including graphene devices considered in Ref. 48, and the localization of acoustics waves in disordered and partially disordered one-dimensional structures.<sup>49–53</sup>

---

### 2.4.7 Conclusion

The term “disorder” usually bears a negative connotation. It is deemed obvious (both in everyday life and in physics and engineering as well) that irregularities are always injurious and detrimental. Contrary to this widely held view, here we argue that if treated properly, disorder can be taken advantage of in numerous technical applications. The unique spectral properties of wave transport in the localized regime presented in this chapter lead one to believe that exploiting randomness can be an effective strategy for creating light-tailoring devices, in particular switchable mirrors and tunable resonant micro- and nano-cavities.

Nowadays photonic crystals are the most extensively used for these purposes. The ability of perfectly periodic structures to manipulate light have long been demonstrated with regard to high-Q cavity resonances, spontaneous emission control, cavity quantum electrodynamical effects, and so on.<sup>45</sup> However, although in laboratory studies photonic crystals perform wholly satisfactorily, practical applications are frequently problematic because of the heavy demands on the accuracy of manufacturing: even small deviations from periodicity could modify dramatically the optical characteristics and hinder the performance of crystal-based devices. That is why significant effort and financial resources are expended to eliminate disorder and to develop pure, ideally regular structures. Yet, a different approach is a possibility: rather than combat the imperfections in periodicity, one can attempt harnessing highly disordered samples as high-Q resonators in optical and microwave switches, filters, and amplifiers. Despite the random character of Anderson modes, their behavior and evolution are rather deterministic, and, therefore, these modes can be used for efficient control of light similar to regular cavity modes.

To suit the optical device designer’s requirements, the transmission should be fast-tunable. Resonant cavities in photonic crystals are created by implanting specially designed defects. Then, the transmission can be controlled by varying the spacing between the given frequency of the incident radiation and the resonant frequency of the cavity, which has to be easily tunable. However, any shift of the spectral line usually requires structural changes of the whole sample,<sup>45,46</sup> which makes such methods practically unusable.

As the localization length (and therefore the typical transmission coefficient) of a 1D random configuration is determined by the power spectrum of disorder, Equation 2.4.8, it is obvious that the frequency spectrum of the transmission can be tailored by varying the spatial structure of the correlation function.<sup>47</sup> Although the physical idea is trivial, its implementation for designing fast-tunable optical devices is problematic because, just as it is in the case of photonic crystals, it needs a rearrangement of the sample as a whole. This however does not mean that unique transport properties of disordered systems cannot be utilized. More sophisticated analysis of the nature of the disorder-induced resonances leads to the conclusion that they are extremely sensitive to changes of the parameters of the medium only inside the effective cavities where eigenmodes are localized. Figure 2.4.13 presents the numerically calculated dependence of the resonant transmission coefficient on the variations of the dielectric constant,  $T(\delta\epsilon)$ , in an area occupying 1/50 of the total length of a random

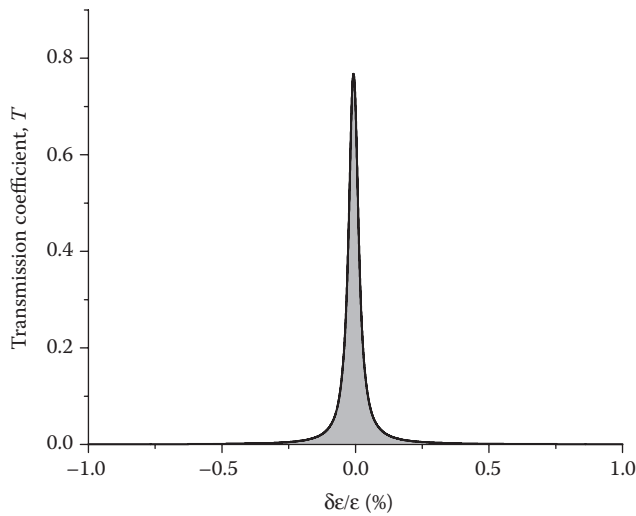


**FIGURE 2.4.13**

Dependence of the resonant transmission coefficient on the variations of the dielectric constant,  $T(\delta\epsilon)$ , in the area occupying  $1/50$  of the total length of a random stack of layers.

stack of layers. It is seen that 1% change in the permittivity only in this area already results in a decrease in  $T$  by the factor  $10^3$ . This example gives good grounds to believe that one can switch a sample from reflection to transmission or tune the emission of a source located inside the sample by external actions; for example, illuminating it by electromagnetic radiation that changes the dielectric constant of the material due to nonlinear effects.

---

## Acknowledgments

V.F. acknowledges partial support from the Israel Science Foundation (Grant No. 894/10). K.Y.B. acknowledges partial support from the European Commission (Marie Curie Action) and Science Foundation Ireland (Grant No. 07/IN.1/I906). F.N. acknowledges partial support from the National Security Agency (NSA), Laboratory Physical Sciences (LPS), Army Research Office (ARO), and National Science Foundation (NSF) (Grant No. 0726909), Grant-in-Aid for Scientific Research (S), MEXT Kakenhi on Quantum Cybernetics, and Funding Program for Innovative R&D on S&T (FIRST).

---

## References

1. P.W. Anderson, *Phys. Rev.* **109**, 1492 (1958).
2. V. Freilikher and S. Gredeskul, *Prog. Opt.* **30**, 37 (1992).
3. P. Cheng, *Introduction to Wave Scattering, Localization and Mesoscopic Phenomena* (Springer-Verlag, Heidelberg, 2006); E. Akkermans and G. Montambaux, *Mesoscopic Physics of Electrons and*

- Photons* (Cambridge University Press, Cambridge, 2007); J.-P. Fouque, J. Garnier, G. Papanicolaou, and K. Solna, *Wave Propagation and Time Reversal in Randomly Layered Media* (Springer Science + Business Media, LLC, New York, 2007); E. Abrahams (ed.), *50 Years of Anderson Localization* (World Scientific, New Jersey/London/Singapore, 2010).
4. I. M. Lifshits, S. A. Gredeskul, and L. A. Pastur, *Introduction to the Theory of Disordered Systems* (Wiley, New York, 1988).
  5. M. V. Berry and S. Klein, *Eur. J. Phys.* **18**, 222 (1997).
  6. U. Frisch, C. Froeschle, J.-P. Scheidecker, and P.-L. Sulem, *Phys. Rev. A* **8**, 1416 (1973); M. Ya. Azbel, *Phys. Rev. B* **28**, 4106 (1983); M. Ya. Azbel and P. Soven, *ibid.* **27**, 831 (1983).
  7. D. S. Wiersma, *Nature* **406**, 132 (2000); V. Milner and A. Genack, *Phys. Rev. Lett.* **94**, 073901 (2005).
  8. H. Cao, Y. G. Zhao, S. T. Ho, E. W. Seelig, Q. H. Wang, and R. P. H. Chang, *Phys. Rev. Lett.* **82**, 2278 (1999).
  9. K. Bliokh, Y. Bliokh, V. Freilikher, A. Genack, and P. Sebbah, *Phys. Rev. Lett.* **101**, 133901 (2008).
  10. N. F. Mott, *Philos. Mag.* **22**, 7 (1970); I. Lifshits, V. Kirpichenkov, *Zh. Eksp. Teor. Fiz.* **77**, 989 (1979) [*Sov. Phys. JETP* **50**, 499 (1979)]; J. Pendry, *Adv. Phys.* **43**, 461 (1994).
  11. J. Pendry, *J. Phys. C* **20**, 733 (1987).
  12. J. Scales, L. Carr, D. McIntosh, V. Freilikher, and Y. Bliokh, *Phys. Rev. B* **76**, 085118 (2007).
  13. I. Shadrivov, K. Bliokh, Y. Bliokh, V. Freilikher, and Y. Kivshar, *Phys. Rev. Lett.* **104**, 123902 (2010).
  14. A. Asatryan, L. Botten, M. Byrne, V. Freilikher, S. Gredeskul, I. Shadrivov, R. McPhedran, and Y. Kivshar, *Phys. Rev. Lett.* **99**, 193902 (2007).
  15. A. Asatryan, L. Botten, M. Byrne, V. Freilikher, S. Gredeskul, I. Shadrivov, R. McPhedran, and Y. Kivshar, *Phys. Rev. B* **81**, 075124 (2010).
  16. A. Asatryan, L. Botten, M. Byrne, V. Freilikher, S. Gredeskul, I. Shadrivov, R. McPhedran, and Y. Kivshar, *Phys. Rev. B* **82**, 205124 (2010).
  17. Y. Bliokh, V. Freilikher, S. Savel'ev, and F. Nori, *Phys. Rev. B* **79**, 075123 (2009).
  18. H. Furstenberg, *Trans. Am. Math. Soc.* **108**, 377 (1963).
  19. V. Kliatskin, *Stochastic Equations and Waves in Randomly Layered Media* (Nauka, Moscow, 1980).
  20. E. Gurevich, Ph.D. thesis, Technion, Haifa, 2011.
  21. E. Gurevich and A. Iomin, *Phys. Rev. E* **83**, 011128 (2011).
  22. P. Anderson, D. Thouless, E. Abrahams, and D. Fisher, *Phys. Rev. B* **22**, 3519 (1980).
  23. V. Baluni and J. Willemsen, *Phys. Rev. A* **31**, 3358 (1985).
  24. K. Bliokh and V. Freilikher, *Phys. Rev. B* **70**, 245121 (2004).
  25. R. Wing, *An Introduction to Invariant Imbedding* (Wiley, New York, 1976).
  26. V. Freilikher, M. Pustilnik, and I. Yurkevich, *Phys. Rev. B* **73**, 810 (1994); **50**, 6017 (1994).
  27. V. Dobrosavljevic, in *50 Years of Anderson Localization*, edited by E. Abrahams (World Scientific, New Jersey/London/Singapore, 2010).
  28. V. Freilikher, M. Pustilnik, and I. Yurkevich, *Phys. Rev. B* **56**, 5974 (1957).
  29. J. Paasschens, T. Misirpashaev, and C. Beenakker, *Phys. Rev. B* **54**, 11887 (1996).
  30. V. Freilikher, B. Lianskii, I. Yurkevich, A. Maradudin, and A. McGurn, *Phys. Rev. E* **51**, 6301 (1995).
  31. K. Bliokh, Y. Bliokh, and V. Freilikher, *J. Opt. Soc. Am. B* **21**, 113 (2004).
  32. K. Bliokh, Y. Bliokh, V. Freilikher, S. Savel'ev, and F. Nori, *Rev. Mod. Phys.* **80**, 1201 (2008).
  33. D. Bohm, *Quantum Theory* (Prentice-Hall, New York, 1952).
  34. B. Payne, J. Andreasen, H. Cao, and A. Yamilov, *Phys. Rev. B* **82**, 104204 (2000).
  35. K. Bliokh, Y. Bliokh, V. Freilikher, A. Genack, B. Hu, and P. Sebbah, *Phys. Rev. Lett.* **97**, 243904 (2006).
  36. J. C. Slater, *Microwave Electronics* (Van Nostrand, Princeton, 1950).
  37. S. Rytov, Y. Kravtsov, and V. Tatarskii, *Principles of Statistical Radiophysics IV: Wave Propagation through Random Media* (Springer-Verlag, Berlin, 1989).
  38. I. Lifshits and V. Kirpichenkov, *Sov. Phys. JETP* **50**, 499 (1979).
  39. J. Bertolotti, S. Gottardo, and D. Wiersma, *Phys. Rev. Lett.* **94**, 113903 (2005).

40. Y. Bliokh, J. Felsteiner, and Y. Slutsker, *Phys. Rev. Lett.* **95**, 165003 (2005).
41. H. Gibbs, S. McCall, and T. Venkatesan, *Phys. Rev. Lett.* **36**, 1135 (1976).
42. M. Feise, I. Shadrivov, Y. Kivshar, and M. Feise, *Phys. Rev. E* **71**, 037602 (2005).
43. V. Cheianov, V. Fal'ko, and B. L. Altshuler, *Science* **315**, 1252 (2007).
44. M. Titov, *Europhys. Lett.* **79**, 17004 (2007).
45. Soon-Hong Kwon, T. Sunner, M. Kamp, and A. Forchel, *Opt. Express* **16**, 11709 (2008).
46. P. Kohli, J. Chatterton, D. Stieler, G. Tuttle, M. Li, X. Hu, Z. Ye, and K. Ho, *Opt. Express* **16**, 1984424 (2008); K. Aoki, D. Guimard, M. Nishioka, M. Nomura, S. Iwamotoi, and Y. Arakawa, *Nat. Photonics* **2**, 688 (2008).
47. F. Izrailev and A. Krokhin, *Phys. Rev. Lett.* **82**, 4062 (1999); U. Kuhl, F. Izrailev, and A. Krokhin, *ibid.* **100**, 126402 (2008); U. Kuhl, F. M. Izrailev, A. Krokhin, and H.-J. Stockmann, *Appl. Phys. Lett.* **77**, 633 (2000); O. Dietz, U. Kuhl, H.-J. Stockmann, N. Makarov, and F. Izrailev, *Phys. Rev. B* **83**, 134203 (2011).
48. A. V. Rozhkov, G. Giavaras, Y. P. Bliokh, V. Freilikher, and F. Nori, *Phys. Reports* **503**, 77 (2011).
49. S. Tamura and F. Nori, *Phys. Rev. B* **40**, 9790 (1989).
50. S. Tamura and F. Nori, *Phys. Rev. B* **41**, 7941 (1990).
51. M. Kolar, M. K. Ali, and F. Nori, *Phys. Rev. B* **43**, 1034 (1991).
52. N. Nishiguchi, S. Tamura, and F. Nori, *Phys. Rev. B* **48**, 2515 (1993).
53. N. Nishiguchi, S. Tamura, and F. Nori, *Phys. Rev. B* **48**, 14426 (1993).

# Optical Properties *of* Photonic Structures

*Interplay of Order and Disorder*

Edited by  
Mikhail F. Limonov  
Richard M. De La Rue



**CRC Press**

Taylor & Francis Group  
Boca Raton London New York

---

CRC Press is an imprint of the  
Taylor & Francis Group, an **informa** business

A TAYLOR & FRANCIS BOOK

Cover image by Diederik and Leonardo Wiersma.

CRC Press  
Taylor & Francis Group  
6000 Broken Sound Parkway NW, Suite 300  
Boca Raton, FL 33487-2742

© 2012 by Taylor & Francis Group, LLC  
CRC Press is an imprint of Taylor & Francis Group, an Informa business

No claim to original U.S. Government works  
Version Date: 20120504

International Standard Book Number-13: 978-1-4398-7192-8 (eBook - PDF)

This book contains information obtained from authentic and highly regarded sources. Reasonable efforts have been made to publish reliable data and information, but the author and publisher cannot assume responsibility for the validity of all materials or the consequences of their use. The authors and publishers have attempted to trace the copyright holders of all material reproduced in this publication and apologize to copyright holders if permission to publish in this form has not been obtained. If any copyright material has not been acknowledged please write and let us know so we may rectify in any future reprint.

Except as permitted under U.S. Copyright Law, no part of this book may be reprinted, reproduced, transmitted, or utilized in any form by any electronic, mechanical, or other means, now known or hereafter invented, including photocopying, microfilming, and recording, or in any information storage or retrieval system, without written permission from the publishers.

For permission to photocopy or use material electronically from this work, please access [www.copyright.com](http://www.copyright.com) (<http://www.copyright.com/>) or contact the Copyright Clearance Center, Inc. (CCC), 222 Rosewood Drive, Danvers, MA 01923, 978-750-8400. CCC is a not-for-profit organization that provides licenses and registration for a variety of users. For organizations that have been granted a photocopy license by the CCC, a separate system of payment has been arranged.

**Trademark Notice:** Product or corporate names may be trademarks or registered trademarks, and are used only for identification and explanation without intent to infringe.

Visit the Taylor & Francis Web site at  
<http://www.taylorandfrancis.com>

and the CRC Press Web site at  
<http://www.crcpress.com>

---

# Contents

---

Preface.....	ix
Editors.....	xi
Contributors.....	xiii

## Section 1 Introduction

<b>1 Introduction.....</b>	<b>3</b>
<i>Sajeev John</i>	

## Section 2 Theory

<b>2.1 Optical Properties of One-Dimensional Disordered Photonic Structures .....</b>	<b>9</b>
<i>Mikhail V. Rybin, Mikhail F. Limonov, Alexander B. Khanikaev, and Costas M. Soukoulis</i>	
<b>2.2 Propagation and Localization of Light in Two-Dimensional Photonic Crystals....</b>	<b>23</b>
<i>Mikhail A. Kaliteevski, Stuart Brand, and Richard A. Abram</i>	
<b>2.3 Modeling the Optical Response of Three-Dimensional Disordered Structures Using the Korringa–Kohn–Rostoker Method .....</b>	<b>39</b>
<i>Gabriel Lozano, Hernán Míguez, Luis A. Dorado, and Ricardo A. Depine</i>	
<b>2.4 Anderson Localization of Light in Layered Dielectric Structures .....</b>	<b>55</b>
<i>Yury Bliokh, Konstantin Y. Bliokh, Valentin Freilikher, and Franco Nori</i>	
<b>2.5 The Disorder Problem for Slow-Light Photonic Crystal Waveguides .....</b>	<b>87</b>
<i>Mark Patterson and Stephen Hughes</i>	
<b>2.6 Quasicrystalline Photonic Structures: Between Order and Disorder .....</b>	<b>131</b>
<i>Alexander N. Poddubny and Eugenyus L. Iochenko</i>	
<b>2.7 Multicomponent Photonic Crystals with Inhomogeneous Scatterers.....</b>	<b>151</b>
<i>Alexander B. Khanikaev, Mikhail V. Rybin, and Mikhail F. Limonov</i>	

## Section 3 Experiment

<b>3.1 Anderson Localization of Light: Disorder-Induced Linear, Nonlinear, and Quantum Phenomena .....</b>	<b>171</b>
<i>Yoav Lahini, Tal Schwartz, Yaron Silberberg, and Mordechai Segev</i>	

<b>3.2 Optical Spectroscopy of Real Three-Dimensional Self-Assembled Photonic Crystals.....</b>	<b>197</b>
<i>Juan F. Galisteo López and Cefe López</i>	
<b>3.3 Photonic Glasses: Fabrication and Optical Properties .....</b>	<b>213</b>
<i>Pedro David Garcia-Fernández, Diederik S. Wiersma, and Cefe López</i>	
<b>3.4 Superdiffusion of Light in Lévy Glasses .....</b>	<b>227</b>
<i>Kevin Vynck, Jacopo Bertolotti, Pierre Barthelemy, and Diederik S. Wiersma</i>	
<b>3.5 Optical Properties of Low-Contrast Opal-Based Photonic Crystals .....</b>	<b>249</b>
<i>Alexander A. Kaplyanskii, Alexander V. Baryshev, Mikhail V. Rybin, Alexander V. Sel'kin, and Mikhail F. Limonov</i>	
<b>3.6 Light and Small-Angle X-Ray Diffraction from Opal-Like Structures: Transition from Two- to Three-Dimensional Regimes and Effects of Disorder .....</b>	<b>275</b>
<i>Anton K. Samusev, Kirill B. Samusev, Ivan S. Sinev, Mikhail V. Rybin, Mikhail F. Limonov, Natalia A. Grigoryeva, Sergey V. Grigoriev, and Andrei V. Petukhov</i>	
<b>3.7 Interplay of Order and Disorder in the High-Energy Optical Response of Three-Dimensional Photonic Crystals.....</b>	<b>301</b>
<i>Gabriel Lozano, Hernán Míguez, Luis A. Dorado, and Ricardo A. Depine</i>	
<b>3.8 Opal-Based Hypersonic Crystals .....</b>	<b>323</b>
<i>Andrey V. Akimov and Alexander B. Pevtsov</i>	
 <b>Section 4 Toward Applications</b>	
<b>4.1 Strong Light Confinement by Perturbed Photonic Crystals and Photonic Amorphous Structures .....</b>	<b>343</b>
<i>Keiichi Edagawa and Masaya Notomi</i>	
<b>4.2 Nonlinear Optics in Silicon Photonic Crystal Nanocavities.....</b>	<b>361</b>
<i>Lucio Claudio Andreani, Paolo Andrich, Matteo Galli, Dario Gerace, Liam O'Faolain, and Thomas F. Krauss</i>	
<b>4.3 Random Lasing Highlighted by <math>\pi</math>-Conjugated Polymer Films .....</b>	<b>379</b>
<i>Randy C. Polson and Z. Valy Vardeny</i>	
<b>4.4 Self-Optimization of Optical Confinement and Lasing Action in Disordered Photonic Crystals.....</b>	<b>395</b>
<i>Alexey Yamilov and Hui Cao</i>	
<b>4.5 Ultrafast All-Optical Switching in Photonic Crystals.....</b>	<b>415</b>
<i>Valery G. Golubev</i>	

<b>4.6 Resonant Light Scattering in Photonic Devices: Role of Defects</b> .....	429
<i>Andrey E. Miroshnichenko and Yuri S. Kivshar</i>	
<b>4.7 Structural Features and Related Optical Responses of Magnetophotonic Crystals</b> .....	445
<i>Mitsuteru Inoue, Alexander V. Baryshev, Alexander M. Merzlikin, Hironaga Uchida, and Alexander B. Khanikaev</i>	
<b>4.8 Inhomogeneous Hybrid Metal–Dielectric Plasmonic–Photonic Crystals</b> .....	469
<i>Sergei G. Romanov</i>	
<b>4.9 Light Propagation in Photonic Crystals Infiltrated with Fluorescent Quantum Dots or Liquid Crystal: Different Dimensionality Analysis</b> .....	487
<i>Rabia Moussa, Alexander Kuznetsov, Ryotaro Ozaki, and Anvar A. Zakhidov</i>	